Some Mean Velocity, Turbulence, and Unsteadiness Characteristics of the VPI & SU Stability Wind Tunnel

by
K. Choi and R. L. Simpson
Aerospace and Ocean Engineering Dept.
VPI & SU

December, 1987.

ABSTRACT

The flow characteristics of the VPI & SU Stability Wind Tunnel with its 6'X6' square test section was investigated. The flow angularities, turbulence intensities are measured across the test section at several flow speeds. The experiment reveals small flow angularities and low turbulence intensities over the test section. Also the space correlations, the time-delayed correlations and the coherence between two streamwise velocity components were measured at two flow speeds of 50 fps and 125 fps. Some discrete unsteadiness frequencies were identified and separated from the raw data to get the final results.

ACKNOWLEDGEMENT

The authors would like to thank Mr. Seungki Ahn for helping to calibrate the hot-wire anemometer, discussing the test results and for every advice he gave. Also it was gratifying to have the help of Mr. Kevin Shinpaugh in achieving the data acquisition program.

TABLE OF CONTENTS

Abstract ---------- i

Acknowledgements ---------- ii

Table of contents ---------- iii

List of Tables ---------- iv

List of Figures ---------- v

Nomenclature ---------- vi

1. Introduction ---------- 1

2. Results from earlier measurements ---------- 2

3. Facility and instrumentation ---------- 3

4. Test procedures ---------- 6

5. Flow survey results and discussion ---------- 9

6. Summary and concluding remarks ---------- 14

References ---------- 15

Appendix ---------- 16

LIST OF TABLES

Table 1.	Previous flow survey on VPI & SU Stability Wind Tunnel with square test section. -------	18
Table 2. (a)	Uncertainties in flow field measurement using a 5-hole yawhead probe. ----------	19
Table 2. (b)	Normalized random error in coherence --------	19
Table 3.	Flow angularities and velocity components across the test section ----------	20
Table 4.	Relative turbulence intensity across the test section ----------	26

LIST OF FIGURES

Figure A-1	Coordinate system ----------	27
Figure A-2	Misalignment angles ----------	27
Figure 1.	Cut-away view of Wind Tunnel ----------	28
Figure 2.(a)	Flow angularity distribution from earlier measurements (Maison,1971) ----------	29
Figure 2.(b)	Turbulence Spectrum at U=49.2 fps ----------	30
Figure 3.	Schematic diagram of instrumentation --------	31
Figure 4.	Location of probe ----------	33
Figure 5.	Velocity vector across the test section -----	35
Figure 6.	Normalized power spectra (U=50 fps) ---------	38
Figure 7.	Normalized power spectra (U=125 fps) --------	43
Figure 8.	Autocorrelation of the streamwise velocity fluctuations ----------	48
Figure 9.	Space correlation of streamwise velocity fluctuations ----------	50
Figure 10.	Coherence of streamwise velocity fluctuations	51

NOMENCLATURE

C_p	pressure coefficient
f	frequency in Hz
F(f)	normalized power spectrum
	$\overline{u^2}_{total} = \overline{u^2}_{turb} + \overline{u^2}_{unsteady} + \overline{u^2}_{noise}$
	$= \overline{u^2}_{total} * \left(\int_0^\infty F(f)df \right)$
G	spectral density function
K	wave number
P_t	stagnation pressure coefficient
q	dynamic pressure
r	distance between probes
R_{uu}	correlation coefficient
T,t	time
u,v,w	fluctuating velocity components
U,V,W	mean velocity components
U_c	convective wave speed
X,Y,Z	wind tunnel coordinate system
X_y, Y_y, Z_y	yaw-head probe coordinate system
α	pitch angle
β	yaw angle
ϕ	roll angle
ε	error
λ	wave length

subscript/superscript

m	misalignment
Y	yaw-head probe
∞	free stream
$\bar{}$	time average
'	root mean square

1. Introduction.

For an ideal wind tunnel test section, the flow outside the boundary layer should have the following characteristics :

a) The velocity profile at each cross section would be uniform
b) There would be no upflow or crossflow.
c) There would be no turbulence.

Since such an ideal flow is difficult to achieve in a wind tunnel, it is important to know the flow quality to determine if it is acceptable for a given tunnel performance and operating cost.

In order to survey the flow characteristics of the V.P.I. & S.U. Stability Wind Tunnel with its 6 ft by 6 ft square test section, the flow angularity distribution across the test section was measured at three different free-stream speeds of 50 fps, 125 fps and 200 fps. Also measurements of turbulence intensities and turbulence power spectral densities and measurements of space correlations, time-delay correlations and the coherence between two streamwise velocity components were performed at two different free stream speeds of 50 fps and 125 fps.

2. Results from earlier measurements.

Mason (1971) measured pitch and yaw angle of the mean flow at U = 70 fps using a 5-hole yawhead probe along the vertical and horizontal center line at two different streamwise locations which he called wing station and section midpoint. As illustrated in Fig. 2 (a), the pitch angles were smaller than $+1^{o}$ and the yaw angles were between -1^{o} and 2^{o} in vertical plane. He also observed small variations in mean flow velocity.

Reynolds (1979) determined that the streamwise velocity fluctuation in this facility was less than 0.04% of the free-stream velocity for the velocity range between 19.7 fps (6 m/sec) and 98.4 fps (30 m/sec) and that the test section had a streamwise pressure gradient $d(C_p)/d(x)$ = -0.0009/ft. Later in 1982, he revealed that variation of the local dynamic pressure was less than 0.05%. Reynolds showed streamwise turbulence energy spectrum for a free-stream velocity of 49.2 fps where the most energetic motions were below 20 Hz (Figure 2 (b)). He also observed an electronic noise at 60 Hz and unsteadiness at 14 Hz due to vibration of motor generator.

According to Lee (1979), an average variation in the mean flow velocity was 0.5% along the vertical and horizontal lines of test section at U = 157 fps.

Previous works are summarized in Table 1.

3. Facility and instrumentation.

3.1 Facility.

The Stability Wind Tunnel at V.P.I. & S.U. is a continuous, single return, closed test section, subsonic wind tunnel with interchangeable round and square test sections. This wind tunnel, constructed, in 1940 was originally a NASA facility located at Langley field in Hampton, Virginia. It was designed to provide a very low turbulence level flow for dynamic stability measurement. In 1958, the wind tunnel was moved to V.P.I & S.U. and recommissioned. A plan view of the facility is shown in Fig. 1.

Although it is a closed loop tunnel, it has an air-exchange tower open to the atmosphere for temperature stabilization. The air-exchange tower is located downstream of the fan and motor assembly and uses a boundary-layer bleed on the entry flow. It turns out that the air-exchange tower provides well-stabilized flow temperature, except for hot summer days.

The square test section is 23 ft long with a constant square cross section of 6 ft by 6 ft. Because of the constant test section area there is no allowance for wall boundary layer growth and a slight negative pressure gradient of C_p = 0.09 % per foot was reported from previous measurements. The test section is enclosed in an air-tight control room to minimize the air leakage into the test section flow. The diffuser angle is 3 degrees and vortex generators are located at the beginning of the diffuser section for efficient diffuser operation.

The flow is driven by a 14.1 ft diameter propeller which has eight constant pitch blades. Power for the fan is provided by a 600 HP d.c. motor. This system has capability of providing a flow in the test section with dynamic pressure up to 40 lb per square foot which corresponds to the free-stream velocity of approximately 220 ft/sec. Test section flow speed is controlled manually by a rheostat control. Electrical power for the d.c. motor is supplied by a Westinghouse Model No. 28767 motor-generator with rotational speed of 900 r.p.m., or 15 Hz.

The turning vanes are located at each corner of the tunnel circuit to provide a uniform flow. These turning vanes have streamlined cross sections and are spaced every 11.8 inches (30 cm) along the diagonal of the corner, except the corner upstream

of the turbulence screens, where the spacing is 3 inches (7.6 cm).

The seven stainless steel wire turbulence screens located in the 18 ft by 18 ft settling chamber are of 0.0079 inch diameter with an open-area ratio of 0.6. Each 18 ft square screen panel is constructed of three 6 ft by 18 ft screens joined together. The two seams in each screen are approximately 0.08 inches wide. The furthest downstream screen panel has horizontal seams and alternate upstream panels are rotated by 90 degrees which results in four horizontal and three vertical sets of seams. The spacing between screens is 5.75 inches. The settling chamber extends past the screens and allows the small-scale eddies to dissipate before entering the nozzle. The nozzle has 9:1 contraction ratio.

3.2 Probe mounting and traverse mechanism.

For flow angularity and power spectra measurements, either a 5-hole yawhead probe or hot-wire probe was mounted on a traverse unit such that it was positioned 14 ft from the front of the test section. In most cases this is the location where the wind tunnel models are mounted. The traverse mechanism is controlled by separate, manually operated control units and spans about 4 ft in both horizontal and vertical directions. The minimum movement is 0.01 inch in horizontal direction and 0.0039 inch in vertical direction. For space correlation and coherence measurements, an additional probe mounting device was needed. Therefore, a hollow bar with streamlined cross section was used to locate a fixed hot-wire probe at the center of cross section while the other probe was mounted on the above mentioned traverse mechanism to provide variable spacings between probes.

3.3 Instrumentation.

3.3.1 Flow angularity measurement.

A schematic diagram of the instrumentation system is illustrated in Fig. 3 (a). During the test a 5-hole yawhead probe (United Sensor model DC 125) was connected to a Scanivalve model D pressure scanner which can scan 48 pressure ports. This pressure scanner is actuated by a pressure scanner controller which is controlled by HP 59306A Relay Actuator. Pressure from each port of pressure scanner is converted to electrical signal

using a Druck (Type PDCR 22) differential pressure transducer whose input range is ± 1 psid. Other monitored quantities were the free stream temperature (Instrulab model 1563 digital thermometer), test section dynamic pressure (a standard pitot-static tube together with a Data Matric model 1173 electric manometer) and test section static pressure (a Valdyne model DB99 digital barometer).

The data channels were scanned by a HP 3495A scanner and a HP 3455A digital voltmeter was used to read the electrical signals. The whole data acquisition system was controlled by a HP 9836 desk top computer. This desk top computer was also used as the real time data processor to monitor the status of mean flow.

3.3.2 Power spectra, correlation and coherence measurements.

A 5-channel Miller-type (1976) hot-wire anemometer (modified by Simpson, et al.(1979)) together with a TSI model 1210-T1.5 Standard Straight Probe was used. This hot-wire probe has a diameter of 0.00015" and is 0.05" long. For measurements that require spacing between probes, two TSI model 1210-T1.5 Straight Probes were used, except for spacings of 0.04 inch (1 mm) and 0.197 inch (5 mm). For these two spacings, TSI model 1244-T1.5 Parallel Sensor Probes were employed. Twelve-volt car batteries with integrated voltage regulators were used instead of the built-in power supply. This helps to get rid of 60 Hz noise and its harmonics from anemometer output signals.

A four channel data 6000 model 611 Universal Wave Form Analyzer and model 681 disk drive by Data Precision were used to get power spectra, correlation coefficients and coherence. Schematic diagram for hot-wire measurements is represented in Fig. 3 (b). Instrumentation for monitoring the free-stream conditions is the same as described for the flow angularity measurements above.

4. Test Procedures.

4.1 Flow angularity measurements.

Measurements at 64 locations at 14 feet from the test section entrance were done at three different free-stream speeds of 50 fps, 125 fps and 200 fps. The measurement grid points were positioned at every 6 inches in both horizontal and vertical directions, as shown in Fig. 4 (a). The pressure from each hole of the yawhead probe was averaged over 25 readings while scanning the pressure ports.

The differential pressure transducer was calibrated by applying known pressure differences of 0 psid and 1 psid. Output from the pressure transducer was assumed to be linear between this pressure range. A model MK 100 Pneumatic Pressure Tester by AMTEK was used to obtain 1 psid. This pressure difference of 1 psid was applied to the sixth port of a pressure scanner to monitor the operation of the pressure transducer during the test. Results of the 5-hole yawhead probe calibration by Sung (1985) were used throughout the data reduction.

Once the yawhead probe was mounted on the traverse unit, misalignment with respect to reference directions were measured and accounted for during the data reduction procedure (see Appendix A).

4.2 Power spectra measurements.

Measurements on 9 locations separated by 1.5 ft as illustrated in Fig. 4 (b) were performed at two different free stream speeds of 50 fps and 125 fps. Linearized outputs from the hot-wire anemometer with an overheat ratio of 1.7 were calibrated in the tunnel test section before the measurements. Linearizer output voltages were measured at several flow speeds in the vicinity of test speed. Then the local slope of the velocity .vs. linearizer output voltage curve was calculated by a linear least square curve fit. The calibration curve had a dispersion from a straight line with a product of moment coefficient in excess of 0.999 and 0.99 for U = 50 fps and 125 fps, respectively. Although the wind tunnel has an air exchange tower, there was a slight temperature increase during the test and it was accounted for by interpolating the slope of calibration curves obtained before and after the test.

The power spectra were obtained from the AC component of linearized output of hot-wire anemometer using the built-in FFT function of the Data 6000 wave form analyzer. From the preliminary measurements no significant energy content was observed at high frequencies. Since most of the turbulence energy of interest occurred in the low frequency range, the data sampling rate was selected as 0.5 KHz at U = 50 fps and 2 KHz at U = 125 fps. This gave a frequency resolution of 0.49 Hz and 1.953 Hz, respectively. The power spectra resulting from a fast Fourier transform of 1204 values of instantaneous velocity were ensemble-averaged over 100 estimates to have total record time of more than 50 seconds.

4.3 Correlation measurements.

The spatial correlation coefficients, $R_{uu}(\Delta r)$, of the streamwise component of velocity fluctuation were obtained from signals at two locations: Δr apart in either vertical or horizontal directions.

$$R_{uu}(\Delta r) = \frac{\overline{u_1 * u_2}}{u'_1 * u'_2}$$

$$\text{where } \overline{u_1 * u_2} = \frac{1}{T}\int_0^T u(r,t)*u(r+\Delta r,t)\,dt$$

$$u'_1 = \sqrt{\frac{1}{T}\int_0^T [u(r,t)]^2\,dt}$$

$$u'_2 = \sqrt{\frac{1}{T}\int_0^T [u(r+\Delta r,t)]^2\,dt}$$

AC components of the hot-wire linearizer output were taken. Then their squared and product terms were ensemble-averaged over 250 time records.

Time-delay autocorrelation of the streamwise component of turbulent fluctuations at the center of the cross section were obtained at free-stream speeds of 50 fps and 125 fps. The autocorrelation feature of Data 6000 wave form analyzer was utilized.

4.4 Coherence measurements.

Bendat and Piersol (1986) presented the coherence function between two signals as

$$\gamma_{12}^2(f) = \frac{|G_{12}(f)|^2}{G_{11}(f) * G_{22}(f)}$$

where $\gamma_{12}^2(f)$ = coherence function

$G_{12}(f)$ = cross-spectra density function

$G_{11}(f)$ = power spectral density function of signal 1

$G_{22}(f)$ = power spectral density function of signal 2

Streamwise components of velocity fluctuation were taken using two hot-wire probes. The spectral density functions were obtained by taking FFTs of these signals. Spectral and cross-spectral density functions were averaged over 100 sets of records and then the coherence function was calculated using the above relation.

5. Flow survey results and discussion.

5.1 Flow angularity measurement.

Velocity vectors on the cross section are plotted in Fig. 5. As we can see from Fig. 5 (a), where U = 50 fps, vertical flow and crossflow are the smallest near the center of the cross section. In Fig. 5 (b) and (c), it is observed that the location with the smallest flow angularity moves progressively from the center of the cross section as the flow speed increases. It is believed that the corner vanes are not sufficient to turn those high speed flows. Flow angularities and corresponding velocity components are presented in Table 3. Flow pitch angles are within $\pm 1^{o}$ along the horizontal center line and flow yaw angles do not exceed $\pm 2^{o}$ across the cross section. This shows good agreement with the results of Mason (1971).

From Fig. 5 and Table 3 the flow angularity becomes larger as the measuring point approaches the test section wall. The effect of the boundary layer growth and that of the traverse mechanism on flow angularity were estimated by assuming: (1) the tunnel wall as a smooth flat plate and (2) the frame of traverse mechanism as two-dimensional circular cylinders. The result from a rough estimation shows total of 0.3^{o} in flow angularity which comes from boundary layer growth (0.1^{o}) and the existence of traverse mechanism (0.2^{o}). This estimation underestimates the flow angularity in some reasons: (1) boundary layer would grow faster than estimated due to some irregularities on the tunnel wall and (2) the traverse mechanism would induce larger flow angularities because its has a more complicated geometry than assumed.

Uncertainties in the flow angularity measurement are considered to arise from two sources : (1) Uncertainties in measuring the yawhead probe misalignments, (2) Uncertainties in the flow field measurement using a yawhead probe (see Appendix for misalignments). Maximum estimated uncertainties from the first source are $\pm 0.5^{o}$ for α_m and ϕ_m, and $\pm 0.3^{o}$ for β_m. These uncertainties have a negligible effect on the relative flow angularities between measuring points especially for small misalignments. Uncertainties from the second source were estimated by Sung (1985) and presented in Table 2 (a). When measuring small flow angles, these uncertainties would be much smaller than those suggested by Sung because his results come from the data for flow angles up to 20 degrees.

5.2 Power spectra measurement.

Turbulence intensities measured at 9 locations are shown in Table 4. Turbulence intensities are extremely low at low test speed (u'/U = 0.05% at U = 50 fps) and become higher with test speed (u'/U = 0.1% at U = 125 fps). However they are still low enough to give a good flow quality. The uncertainty in turbulence intensity was ±0.0001 for U = 50 fps and +0.0003 for U = 125 fps. Although the turbulence intensity becomes slightly higher as the measuring point approaches the test section walls and corners, it is still very low.

Normalized power spectra are illustrated in Fig. 6 and 7, which show most of the energy below 50 Hz for U = 50 fps and below 1000 Hz for U = 125 fps. Reynolds (1982) reported the most energetic motions below the frequency of 20 Hz when U_∞ = 49.2 fps. Current data supports Reynolds' results except the 15 Hz unsteadiness is somewhat more discrete here than shown by Reynolds. Some peaks are seen in the power spectra :

a) The flow is driven by an eight-bladed fan rotating at 137 r.p.m. (U = 50 fps) and 337 r.p.m. (U = 125 fps). This fan produces the blade passing frequency of 18 Hz at U = 50 fps and 45 Hz at U = 125 fps.

b) A peak at low frequency, between 3 Hz and 4 Hz, is thought to come from the vibration of the wind tunnel structure itself.

c) Some small peaks with frequencies higher than 100 Hz are due to the vibration of the probe stem.

d) A Westinghouse Model No.28767 motor-generator with its rotational speed of 900 r.p.m. produces 15 Hz vibration in the test section.

Above mentioned peaks in power spectra due to unsteadiness and the high frequency noise of the hot-wire are not counted in calculating turbulence intensities, i.e.

$$\text{(turbulence intensity)} = [\overline{u^2}_{\text{total}} - \overline{u^2}_{\text{unsteady}} - \overline{u^2}_{\text{noise}}]^{1/2} / U$$

Assuming that $U_c \approx U_\infty$ for a non-shear flow, power spectra shown in Fig. 6 and 7 can be represented as a function of wave number, K, as follows

$$\lambda = \frac{U_c}{f}$$

where λ : wave length
U_c : convective wave speed
f : frequency

Therefore,

$$K = \frac{2\pi}{\lambda} = \frac{2\pi f}{U_\infty}$$

5.3 Correlation measurement.

Time-delayed autocorrelation coefficients of streamwise velocity components at the center of the test section are shown in Fig. 8. When U = 50 fps, the autocorrelation decreases from unity at zero time delay to 0.269 at 0.2 msec time delay. The frequency of large time-delay autocorrelation oscillation is about 15 Hz, which corresponds to the spectral peak due to unsteadiness shown in Figures 6 (a - i). At a higher test speed (U = 125 fps), the autocorrelation coefficient drops from unity at zero time delay to 0.721 at 0.2 msec time delay. Then it decreases to zero at 10 msec time delay. The 75 Hz oscillation at large time-delay comes from the spectral peak shown in Figures 7 (a -i).

Space correlation coefficients are plotted in Fig. 9. Although it is not presented in the figure, the correlation coefficient did not decay much as the spacing between probes was increased. This is due to the unsteadiness in the flow which can be corrected as follows;

$$\overline{u_{turb1} * u_{turb2}} = \overline{u_1} * \overline{u_2} - \overline{u^2}_{unsteady}$$

$$\overline{u^2}_{turb1} = \overline{u^2}_1 - \overline{u^2}_{unsteady}$$

$$\overline{u^2}_{turb2} = \overline{u^2}_2 - \overline{u^2}_{unsteady}$$

where $u_1 = u_{turb1} + u_{unsteady}$

$u_2 = u_{turb2} + u_{unsteady}$

Therefore,

$$(R_{uu})_{corrected} = \frac{u_{turb1} * u_{turb2}}{\sqrt{\overline{u^2}_{turb1} * \overline{u^2}_{turb2}}}$$

Fig. 9 shows spatial correlation coefficients after applying the above correction. In Fig. 9 (a), correlation curve decreases faster for a higher test speed. This indicates that at the higher test speed, the high frequency motions by small eddies contributes more to the flow. The same conclusion can be extracted from the power spectra plot which has a fuller shape in the high frequency region at U = 125 fps. The uncertainty in the space correlation coefficient is estimated as ± 0.043.

The integral length scale gives the average size of the eddies and is expressed as

$$L = \int_0^\infty R_{uu}(\Delta r)\ dr$$

After performing the integration using the curves in Fig. 9, we have:

$(L_z)_{u=50fps}$ = 2.2 inch

$(L_z)_{u=125fps}$ = 1.1 inch

$(L_y)_{u=50fps}$ = 4.8 inch

$(L_y)_{u=125fps}$ = 1.0 inch

Here a linear variation of $R_{uu}(\Delta r)$ between 1.0 at $\Delta r=0$ and the value at $\Delta r=1$ mm was used in the integration. The average size of the eddies are smaller for the flow with higher speed.

5.4 Coherence measurement.

The Coherence between streamwise velocity fluctuation from two probes with spacings in either y- or z-direction is shown in Fig. 10 . In Fig. 10 (a) and (b), where U = 50 fps, strong coherence is observed at 15 Hz which is due to the unsteadiness from the fan blade and motor generator. Notice that the coherence from unsteadiness does not decay with the separation distance between probes. Also unexplainably poor coherence is observed at the low frequency range for the closest two separation distances where the most coherent results were expected. For the spacings larger than 0.87 inch, coherence for low frequency motions decay with separation distance. However, no noticeable decay is observed in the frequency range above 20 Hz because the energy contained in this frequency motion is too low to make a contribution to coherence. In Fig. 10 (c) and (d), where U = 125 fps, some narrow band peaks due to unsteadiness are observed and the coherence shows a tendency to decay with separation distance. For this flow, the fan blade passing frequency was 45 Hz. In a homogeneous isotropic turbulent flow, zero coherence between the two probes is expected whenever the separation distance is greater than about twice the integral length scale of the energetic eddies. However, the experiment shows a nonzero broadband coherence which is likely to result from all sources of unsteadiness in the flow and experimental uncertainties. Bias error in coherence measurement was negligible due to a large number of averaged records. The normalized random error in coherence is presented in Table 2 (b).

6. Summary and Concluding Remarks

a) Available previous measurements on the flow quality for the VPI & SU Stability wind tunnel are gathered and summarized.

b) Flow angularity and turbulence intensity are measured at two flow speeds. These measurements are distributed over cross section whereas previous measurements were along a center line or at the center of the cross section. Flow angularities in yaw and pitch are less than $\pm 2^{o}$ and the position of minimum flow angularity deviates from the center of the cross section as the flow speed increases. The turbulence intensity is as low as 0.05% at U = 50 fps and uniform across the cross section. Turbulence intensity increases to about 0.1% at U = 125 fps.

c) The unsteady flow signals and true turbulent signals were separated to correct the spatial correlation coefficient and turbulent intensities.

d) Integral length scale in vertical direction was estimated as 3.46 inch for U = 50 fps and 0.86 inch for U = 125 fps. For horizontal direction, integral length scale was 4.83 inch for U = 50 fps and 1.0 inch for U = 125 fps.

e) The frequency bandwidth which contribute the turbulence intensity is below 40 Hz for U = 50 fps and below 200 Hz for U = 125 fps. Also, some discrete unsteadiness frequencies were observed: the eight-bladed fan produces 18 Hz and 45 Hz unsteadiness at U = 50 fps and 125 fps respectively; the vibration of wind tunnel produces 3-4 Hz unsteadiness; small peaks with frequencies higher than 100 Hz comes from the vibration of hot-wire probe stem; the motor generator causes 15 Hz unsteadiness.

- REFERENCES -

1. Bendat, J.S., and Piersol, A.G., "Random Data", John Wiley & Sons, 1986.

2. Lee, H., "Mean and Turbulent Flow Measurement in the Near Wake of A Self-Propelled Submarine- and/or Airship-like Model at Pitch or Yaw", M.S. Thesis, VPI & SU, 1980

3. Mason, W.H., "Farfield Structure of an Aircraft Trailing Vortex", M.S. Thesis, VPI & SU, 1971

4. Miller, J.A., "Simple Linearized Hot-Wire Anemometer," Journal of Fluids Engineering, Vol.98, pp.550-557

5. Rae, W.H., and Pope, A., "Low-Speed Wind Tunnel Testing", John Wiley & Sons, 1984

6. Reynolds, G.A., "Experiments on the Stability of the Blasius Boundary-Layer", M.S. Thesis, VPI & SU, 1979

7. Reynolds, G.A., "Experiments on the Stability of the Flat-Plate Boundary-Layer with Suction", Ph.D. Dissertation, VPI & SU, 1982

8. Simpson, R.L., Heizer, K.W., and Nasburg, R.E., "Performance Characteristics of a Simple Linearized Hot-Wire Anemometer", Journal of Fluids Engineering, Vol. 101, pp.381-382, 1979

9. Sung, B., "Analysis of the Vortical Flow Around a 60 Degree Delta Wing with Vortex Flap", Ph.D. Dissertation, VPI & SU, 1985

APPENDIX A

-- Yawhead Probe Misalignment and Their Compensation --

The right hand orthogonal coordinate system used in this report is presented in Fig. A-1. The x-axis lies in the horizontal plane with positive direction to the downstream. The z- axis runs in vertical direction with positive direction upward and the y-axis is perpendicular to the test section side wall.

Misalignment angles of yawhead probe with respect to the reference axes are shown in Fig. A-2. Angles as shown in the figure are considered as positive. Once the yawhead probe was mounted on the traverse mechanism, these misalignment angles were measured:

a) Misalignment in pitch (α_m) ; Angle between X-axis and probe stem makes this angle. Inclinometer and cathetometer were used to measure pitch angle.

b) Misalignment in roll (ϕ_m) ; A hypothetical line which passes top and bottom hole of yawhead probe and Z-axis makes roll angle. Cathetometer was used.

c) Misalignment in yaw (β_m) ; Two points on the stem of yawhead probe were selected. Then the distances from tunnel side wall to each of these points were measured. These two distances together with the distance between two points in X-direction gives the angle β_m.

There is another source of misalignments because the yawhead probe could have a different attitude on each measuring position while travelling along the traverse mechanism. Attitude change in pitch and roll were also measured and compensated together with the above mentioned misalignments.

Velocity components; U_y, V_y and W_y; with respect to the yawhead probe were measured during the test and transformed to the velocity components in the reference axes system using the following relations.

$$U = (\cos\alpha_m + \cos\beta_m)*U_y + (\sin\alpha_m*\sin\phi_m - \cos\alpha_m*\sin\beta_m*\cos\phi_m)*V_y + (\cos\alpha_m*\sin\beta_m*\sin\phi_m + \sin\alpha_m*\cos\phi_m)*W_y$$

$$V = \sin\beta_m * U_y + \cos\beta_m *\sin\phi_m * V_y - \cos\beta_m * \sin\phi_m * W_y$$

$$W = -\sin\alpha_m*\cos\beta_m * U_y + (\sin\alpha_m*\sin\beta_m*\cos\phi_m + \cos\alpha_m*\sin\phi_m)*V_y + (\cos\alpha_m*\cos\phi_m - \sin\alpha_m*\sin\beta_m*\sin\phi_m)*W_y$$

Table 1. Previous Flow Survey on VPI & SU Stability W/T with Square Test Section

	Name	Mean Flow Velocity	Results	Comments
Total velocity variation	Mason (1971)	-	Low	along vertical & horizontal center lines
	Lee (1979)	157 fps 47m/s	0.5% of U_∞ (average)	"
Flow angularity	Mason (1971)	70 fps	$-1^o < \alpha < 1^o$ $-1^o < \beta < 2^o$	vertical center line horizontal center line
Axial pressure gradient	Lee (1983)	157 fps	negligible	
	Reynolds (1982)	-	$d(C_p)/dx = -.003$/meter	
Variation in local dynamic pressure	Reynolds (1982)	-	less than .05%	
	Lee (1979)	157 fps	less than .05cm H_2O	
Streamwise vel.fluctuation $\left\|\frac{u'}{U_\infty}\right\|$	Reynolds	9m/sec 10m/sec 15m/sec 20m/sec 30m/sec	.018% .018% .022% .028% .045%	

50 - 75 m/s
125 - 37.5 m/s

$\delta\alpha$(deg)	$\delta\beta$(deg)	δP_t(%)	δq(%)
0.51	0.56	1.33	1.34

Table 2.a) Uncertainties in flow field measurement using a 5-hole yawhead probe

γ^2_{12}	0.2	0.4	0.6	0.8	1.0
$\varepsilon(\gamma^2_{12})$	$\pm$0.253	$\pm$0.134	$\pm$0.073	$\pm$0.032	0.0

Table 2.b) Normalized random error in coherence

Y (FT)	Z (FT)	U (FPS)	V (FPS)	W (FPS)	ALPHA (DEG)	BETA (DEG)
1.75	-1.5	49.442	-0.260	0.943	1.092	-0.301
	-1.0	49.559	-0.699	0.776	0.896	-0.808
	-0.5	49.341	-0.723	0.428	0.497	-0.840
	0.0	49.991	-0.623	0.311	0.356	-0.714
	0.5	49.516	-1.036	-0.261	-0.302	-1.198
	1.0	49.614	-0.884	-0.572	-0.660	-1.021
	1.5	49.541	-0.895	-1.354	-1.566	-1.035
	2.0	49.162	-1.008	-1.541	-1.796	-1.174
1.25	-1.5	49.730	-0.381	0.910	1.048	-0.439
	-1.0	49.649	-0.761	0.599	0.691	-0.878
	-0.5	49.682	-0.630	0.458	0.528	-0.726
	0.0	50.029	-0.602	0.361	0.414	-0.690
	0.5	50.194	-0.626	0.105	0.120	-0.714
	1.0	49.924	-0.905	-0.780	-0.895	-1.038
	1.5	49.790	-0.822	-1.093	-1.258	-0.945
	2.0	49.653	-0.772	-1.449	-1.672	-0.891
0.75	-1.5	49.761	-0.068	0.877	1.010	-0.079
	-1.0	49.876	-0.235	0.428	0.492	-0.270
	-0.5	50.132	-0.409	0.538	0.615	-0.468
	0.0	49.952	-0.321	-0.057	-0.065	-0.368
	0.5	50.159	-0.512	-0.092	-0.105	-0.584
	1.0	49.975	-0.496	-0.485	-0.556	-0.569
	1.5	50.008	-0.592	-1.191	-1.364	-0.678
	2.0	49.538	-0.629	-1.688	-1.952	-0.728
0.25	-1.5	49.805	0.020	0.953	1.096	0.022
	-1.0	50.064	-0.177	0.707	0.809	-0.203
	-0.5	49.935	-0.206	0.278	0.319	-0.237
	0.0	50.082	-0.154	0.312	0.357	-0.176
	0.5	50.246	-0.379	-0.155	-0.177	-0.432
	1.0	50.129	-0.518	-0.600	-0.686	-0.592
	1.5	50.225	-0.451	-0.725	-0.827	-0.514
	2.0	49.746	-0.516	-1.678	-1.932	-0.594

Table 3.a) Flow angularities and velocity components across the test section (U = 50 fps).

Y (FT)	Z (FT)	U (FPS)	V (FPS)	W (FPS)	ALPHA (DEG)	BETA (DEG)
-0.25	-1.5	49.678	0.297	0.746	0.861	0.343
	-1.0	50.333	0.115	0.783	0.891	0.130
	-0.5	49.909	-0.135	0.523	0.600	-0.155
	0.0	50.311	-0.025	0.188	0.214	-0.029
	0.5	50.335	-0.196	-0.225	-0.256	-0.223
	1.0	50.260	-0.071	-0.465	-0.530	-0.081
	1.5	50.024	-0.131	-1.130	-1.295	-0.150
	2.0	49.626	-0.280	-1.597	-1.844	-0.323
-0.75	-1.5	49.645	0.448	0.932	1.075	0.518
	-1.0	49.891	0.468	0.876	1.007	0.538
	-0.5	50.199	0.324	0.356	0.407	0.370
	0.0	50.211	0.357	0.181	0.206	0.407
	0.5	50.244	0.185	-0.298	-0.340	0.211
	1.0	50.210	0.101	-0.488	-0.557	0.116
	1.5	49.979	0.032	-0.956	-1.095	0.037
	2.0	49.534	-0.201	-1.643	-1.900	-0.233
-1.25	-1.5	49.593	0.752	1.101	1.271	0.869
	-1.0	49.584	0.657	0.417	0.482	0.759
	-0.5	49.707	0.646	0.436	0.503	0.744
	0.0	49.850	0.512	0.022	0.025	0.588
	0.5	49.847	0.483	0.005	0.006	0.555
	1.0	49.818	0.511	-0.833	-0.958	0.587
	1.5	49.820	0.502	-1.003	-1.154	0.577
	2.0	49.476	0.244	-1.543	-1.786	0.282
-1.75	-1.5	49.256	0.909	1.102	1.281	1.027
	-1.0	49.240	0.822	0.700	0.815	0.956
	-0.5	49.384	0.925	0.571	0.662	1.074
	0.0	49.296	0.877	0.257	0.298	1.020
	0.5	49.663	0.702	-0.111	-0.128	0.810
	1.0	49.446	0.766	-0.441	-0.511	0.888
	1.5	49.476	0.518	-0.816	-0.945	0.600
	2.0	49.095	0.492	-1.021	-1.192	0.574

Table 3.a) Continued

Y (FT)	Z (FT)	U (FPS)	V (FPS)	W (FPS)	ALPHA (DEG)	BETA (DEG)
1.75	-1.5	122.131	-1.801	1.696	0.796	-0.845
	-1.0	123.557	-1.702	1.676	0.777	-0.789
	-0.5	123.717	-1.728	0.874	0.405	-0.800
	0.0	123.783	-1.985	0.530	0.245	-0.919
	0.5	123.742	-1.903	-0.323	-0.150	-0.881
	1.0	123.883	-2.299	-1.505	-0.696	-1.063
	1.5	123.500	-2.362	-3.505	-1.626	-1.096
	2.0	122.541	-2.232	-4.230	-1.977	-1.043
1.25	-1.5	122.920	-1.092	2.628	1.225	-0.509
	-1.0	123.919	-1.283	1.821	0.842	-0.593
	-0.5	124.600	-1.347	1.212	0.557	-0.619
	0.0	124.866	-1.584	0.399	0.183	-0.727
	0.5	124.637	-1.929	-0.497	-0.228	-0.887
	1.0	124.975	-2.020	-1.784	-0.818	-0.926
	1.5	124.268	-1.978	-3.227	-1.487	-0.912
	2.0	123.167	-2.103	-4.284	-1.992	-0.978
0.75	-1.5	124.164	-0.878	2.139	0.987	-0.405
	-1.0	124.103	-0.847	1.819	0.840	-0.391
	-0.5	124.880	-1.106	1.387	0.636	-0.508
	0.0	124.846	-1.301	0.523	0.240	-0.597
	0.5	124.842	-1.667	-0.547	-0.251	-0.765
	1.0	125.198	-1.630	-1.711	-0.783	-0.746
	1.5	124.514	-1.619	-3.117	-1.434	-0.745
	2.0	123.629	-1.737	-4.408	-2.042	-0.805
0.25	-1.5	124.813	-0.372	2.462	1.130	-0.171
	-1.0	124.732	-0.261	1.905	0.875	-0.120
	-0.5	125.183	-0.455	1.054	0.482	-0.208
	0.0	125.274	-0.851	0.292	0.134	-0.389
	0.5	124.975	-1.009	-0.507	-0.232	-0.463
	1.0	125.251	-1.299	-1.496	-0.684	-0.594
	1.5	125.174	-1.021	-3.000	-1.373	-0.467
	2.0	123.693	-1.235	-4.637	-2.147	-0.572

Table 3.b) Flow angularities and velocity components across the test section (U = 125 fps).

Y (FT)	Z (FT)	U (FPS)	V (FPS)	W (FPS)	ALPHA (DEG)	BETA (DEG)
-0.25	-1.5	124.269	0.742	2.637	1.215	0.342
	-1.0	125.078	0.241	2.069	0.948	0.110
	-0.5	125.151	0.018	1.241	0.568	0.008
	0.0	125.429	-0.201	0.476	0.217	-0.092
	0.5	125.370	-0.291	-0.482	-0.220	-0.133
	1.0	125.232	-0.482	-1.418	-0.649	-0.221
	1.5	125.117	-0.580	-2.940	-1.346	-0.266
	2.0	124.112	-0.707	-4.242	-1.957	-0.327
-0.75	-1.5	123.872	1.209	2.686	1.242	0.559
	-1.0	124.710	0.901	2.003	0.920	0.414
	-0.5	124.713	0.556	1.166	0.536	0.255
	0.0	125.188	0.523	0.487	0.223	0.239
	0.5	125.436	0.297	-0.350	-0.160	0.136
	1.0	125.193	0.363	-1.542	-0.706	0.166
	1.5	124.786	0.194	-2.937	-1.348	0.089
	2.0	123.506	0.044	-4.222	-1.958	0.020
-1.25	-1.5	123.465	1.957	2.733	1.268	0.908
	-1.0	124.552	1.591	2.176	1.001	0.732
	-0.5	124.702	1.444	1.288	0.592	0.663
	0.0	124.917	1.158	0.347	0.159	0.531
	0.5	124.593	0.999	-0.386	-0.177	0.459
	1.0	124.866	1.215	-1.559	-0.716	0.557
	1.5	124.512	0.990	-2.957	-1.360	0.456
	2.0	123.428	0.425	-4.454	-2.067	0.197
-1.75	-1.5	122.488	2.690	2.618	1.224	1.258
	-1.0	123.294	2.334	2.012	0.935	1.084
	-0.5	123.339	2.057	1.639	0.761	0.955
	0.0	123.893	1.771	0.567	0.262	0.819
	0.5	123.928	1.392	-0.236	-0.109	0.644
	1.0	123.600	1.934	-0.940	-0.436	0.897
	1.5	123.428	1.574	-2.235	-1.037	0.730
	2.0	122.301	1.030	-3.716	-1.740	0.483

Table 3.b) Continued

Y (FT)	Z (FT)	U (FPS)	V (FPS)	W (FPS)	ALPHA (DEG)	BETA (DEG)
1.75	-1.5	196.041	-3.123	4.029	1.177	-0.913
	-1.0	197.609	-3.625	3.487	1.011	-1.051
	-0.5	198.078	-3.912	2.520	0.729	-1.131
	0.0	197.862	-4.856	1.263	0.366	-1.406
	0.5	197.568	-5.275	-0.156	-0.045	-1.529
	1.0	197.978	-5.836	-2.643	-0.765	-1.689
	1.5	196.986	-6.238	-5.210	-1.515	-1.814
	2.0	195.844	-6.078	-6.255	-1.829	-1.778
1.25	-1.5	197.675	-2.986	5.022	1.455	-0.865
	-1.0	198.614	-4.036	4.126	1.190	-1.164
	-0.5	200.556	-3.124	3.531	1.009	-0.892
	0.0	198.837	-4.578	2.502	0.721	-1.319
	0.5	198.985	-4.579	0.454	0.131	-1.318
	1.0	198.991	-6.009	-1.555	-0.448	-1.730
	1.5	198.802	-5.037	-4.331	-1.248	-1.451
	2.0	197.230	-6.072	-6.434	-1.868	-1.763
0.75	-1.5	198.275	-1.344	4.956	1.432	-0.388
	-1.0	199.666	-1.703	5.626	1.614	-0.489
	-0.5	199.687	-2.815	3.592	1.030	-0.808
	0.0	200.012	-3.748	1.967	0.563	-1.074
	0.5	200.166	-4.638	0.473	0.136	-1.327
	1.0	199.191	-4.308	-0.923	-0.265	-1.239
	1.5	200.282	-5.232	-3.750	-1.073	-1.496
	2.0	196.481	-3.608	-5.751	-1.677	-1.052
0.25	-1.5	197.533	0.218	6.041	1.752	0.063
	-1.0	199.400	-0.743	4.056	1.165	-0.213
	-0.5	199.277	-1.938	4.029	1.158	-0.557
	0.0	201.140	-2.775	2.289	0.652	-0.790
	0.5	200.688	-3.623	1.414	0.404	-1.034
	1.0	199.776	-3.831	-0.995	-0.285	-1.099
	1.5	199.997	-3.877	-3.046	-0.872	-1.111
	2.0	199.553	-4.175	-5.712	-1.656	-1.211

Table 3.c) Flow angularities and velocity components across the test section (U = 200 fps).

Y (FT)	Z (FT)	U (FPS)	V (FPS)	W (FPS)	ALPHA (DEG)	BETA (DEG)
-0.25	-1.5	198.833	0.817	6.969	2.007	0.235
	-1.0	198.863	-0.441	5.669	1.633	-0.127
	-0.5	199.216	-0.016	4.755	1.367	-0.005
	0.0	199.861	-0.998	2.652	0.760	-0.286
	0.5	199.739	-2.106	1.817	0.521	-0.604
	1.0	199.773	-2.352	-0.170	-0.049	-0.674
	1.5	200.153	-2.375	-2.503	-0.716	-0.680
	2.0	199.361	-2.803	-5.073	-1.458	-0.806
-0.75	-1.5	198.067	2.515	6.953	2.011	0.727
	-1.0	199.330	1.637	5.716	1.643	0.471
	-0.5	200.339	1.394	4.834	1.382	0.399
	0.0	199.955	0.255	4.088	1.171	0.073
	0.5	200.610	-0.721	1.979	0.565	-0.206
	1.0	199.229	-0.727	0.015	0.004	-0.209
	1.5	198.668	-1.385	-1.759	-0.507	-0.399
	2.0	197.359	-2.118	-4.787	-1.389	-0.615
-1.25	-1.5	197.372	3.490	7.697	2.233	1.013
	-1.0	198.477	3.268	5.879	1.697	0.943
	-0.5	198.919	1.665	6.129	1.765	0.480
	0.0	199.305	1.435	3.624	1.042	0.413
	0.5	199.559	1.583	2.083	0.598	0.454
	1.0	199.966	1.177	0.806	0.231	0.337
	1.5	198.795	0.711	-2.217	-0.639	0.205
	2.0	197.492	-0.244	-4.013	-1.164	-0.071
-1.75	-1.5	196.989	4.507	7.106	2.066	1.311
	-1.0	196.971	4.504	7.594	2.208	1.310
	-0.5	196.775	3.566	5.823	1.695	1.038
	0.0	197.515	2.908	4.050	1.175	0.844
	0.5	197.576	1.760	2.849	0.826	0.510
	1.0	196.844	2.459	1.414	0.416	0.716
	1.5	196.540	1.560	-1.099	-0.320	0.455
	2.0	195.276	0.633	-3.390	-0.995	0.186

Table 3.c) Continued

Z \ Y	-1.5 FT	0.0 FT	1.5 FT
1.5 FT	0.045%	0.039%	0.053%
0.0 FT	0.038%	0.041%	0.043%
-1.5 FT	0.042%	0.036%	0.052%

Table 4. (a) Relative turbulence intensity across the test section (test speed = 50 fps)

Z \ Y	-1.5 FT	0.0 FT	1.5 FT
1.5 FT	0.102%	0.093%	0.107%
0.0 FT	0.104%	0.072%	0.115%
-1.5 FT	0.101%	0.099%	0.121%

Table 4. (b) Relative turbulence intensity across the test section (test speed = 125 fps)

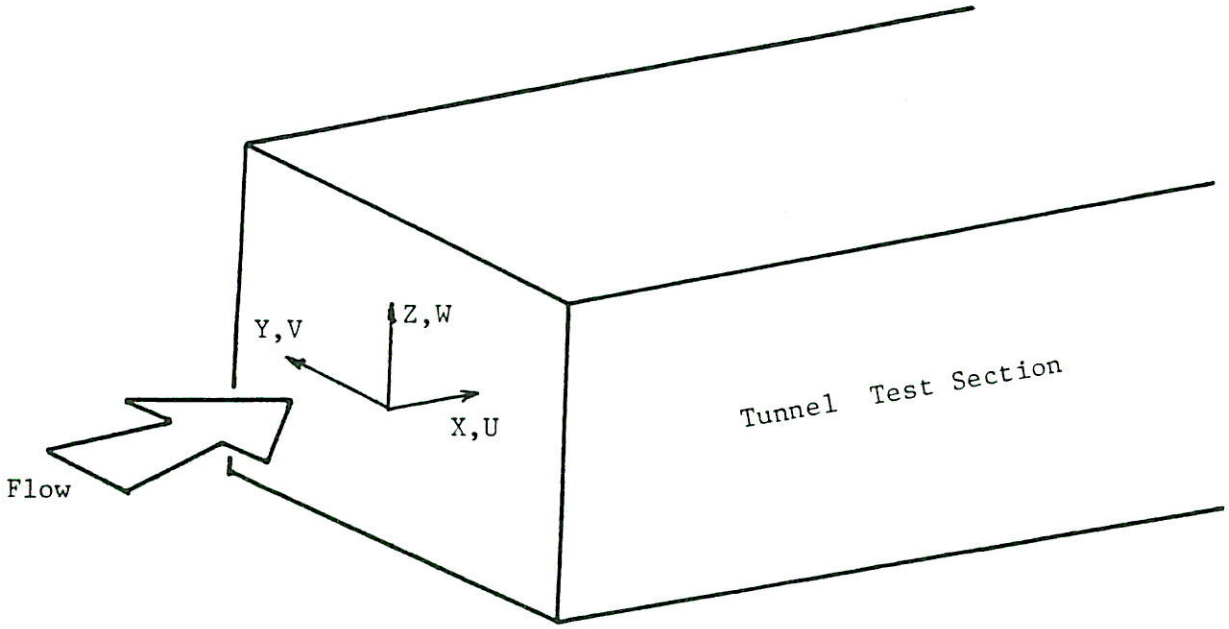

Fig. A-1. Coordinate System

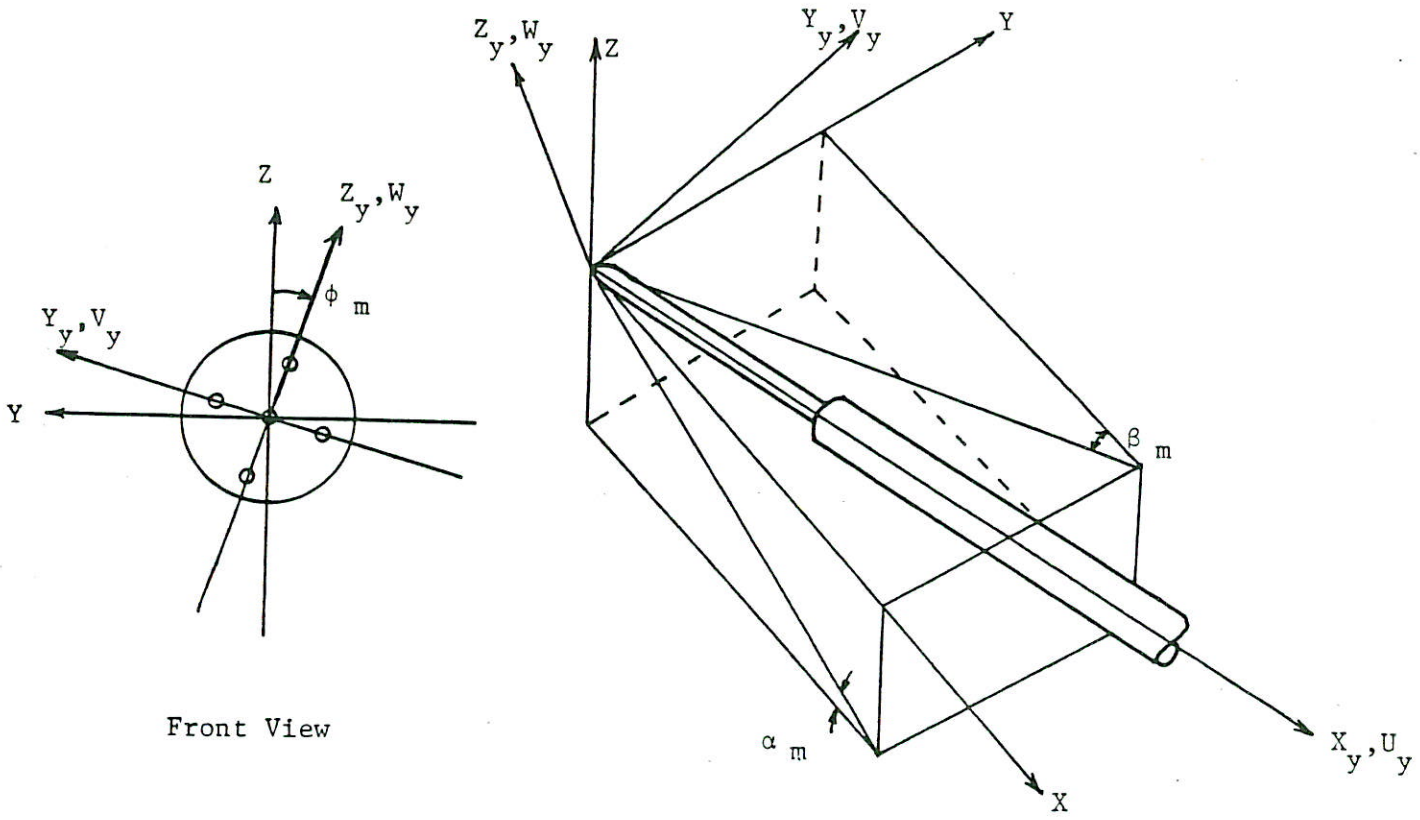

Fig. A-2. Misalignment Angles

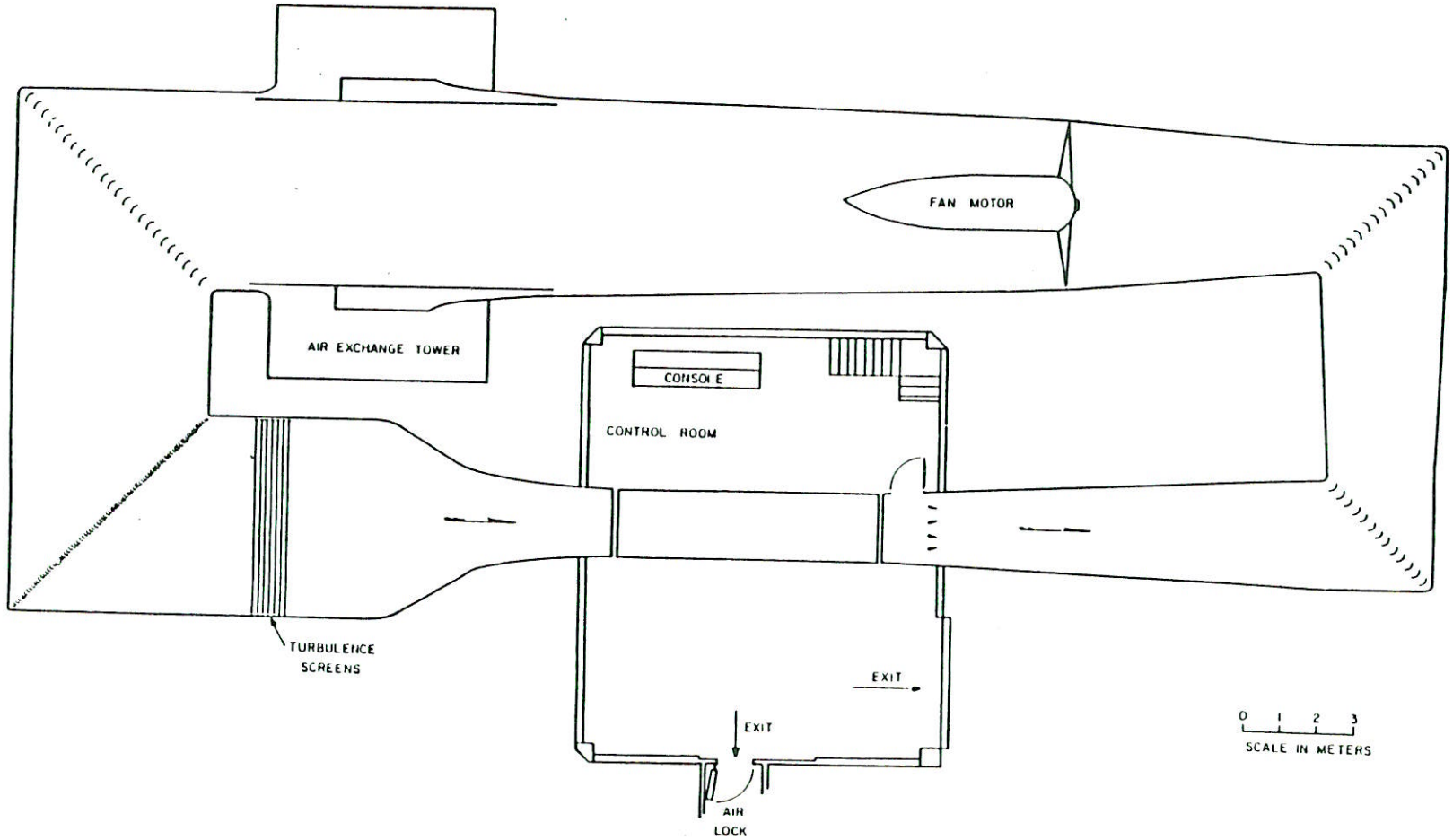

Fig. 1. Cut-away view of Wind Tunnel

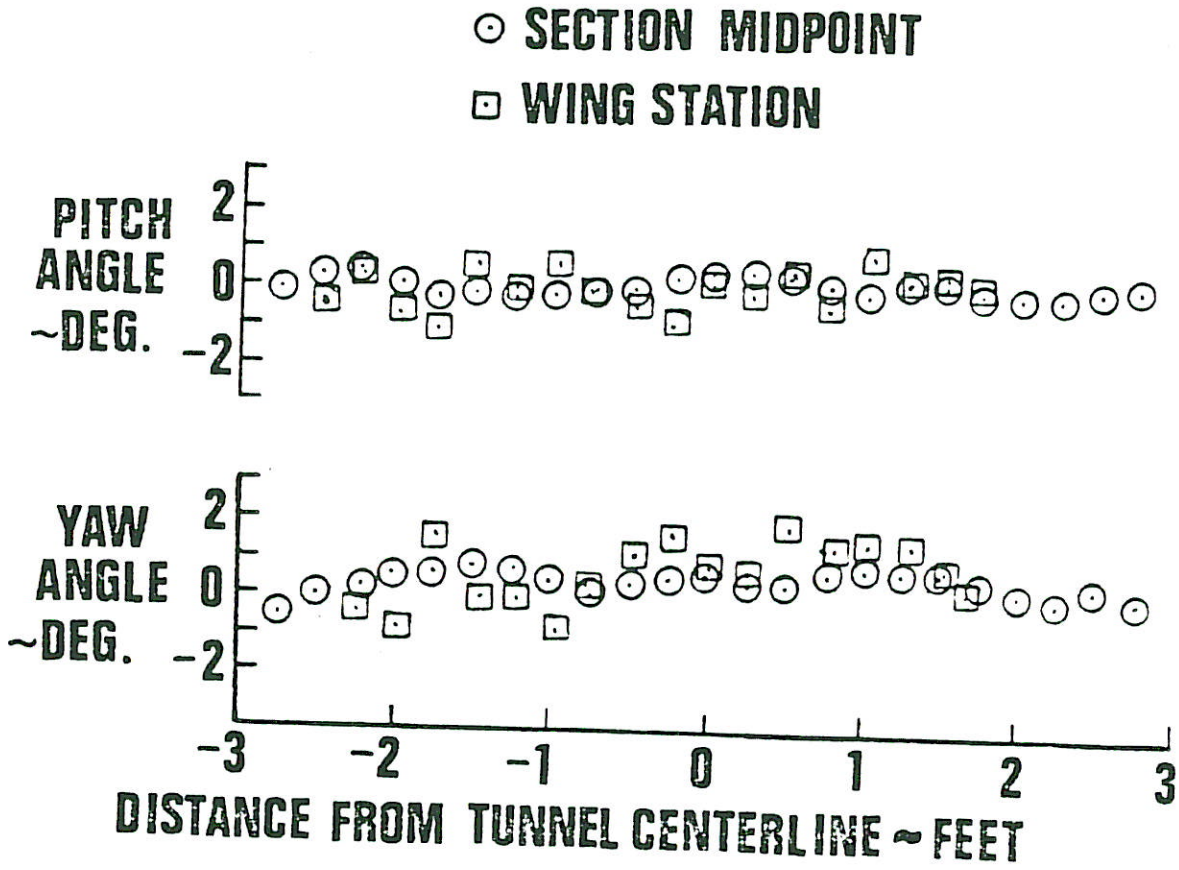

Fig. 2 a). Flow angularity distribution from earlier measurements (Mason, 1971).

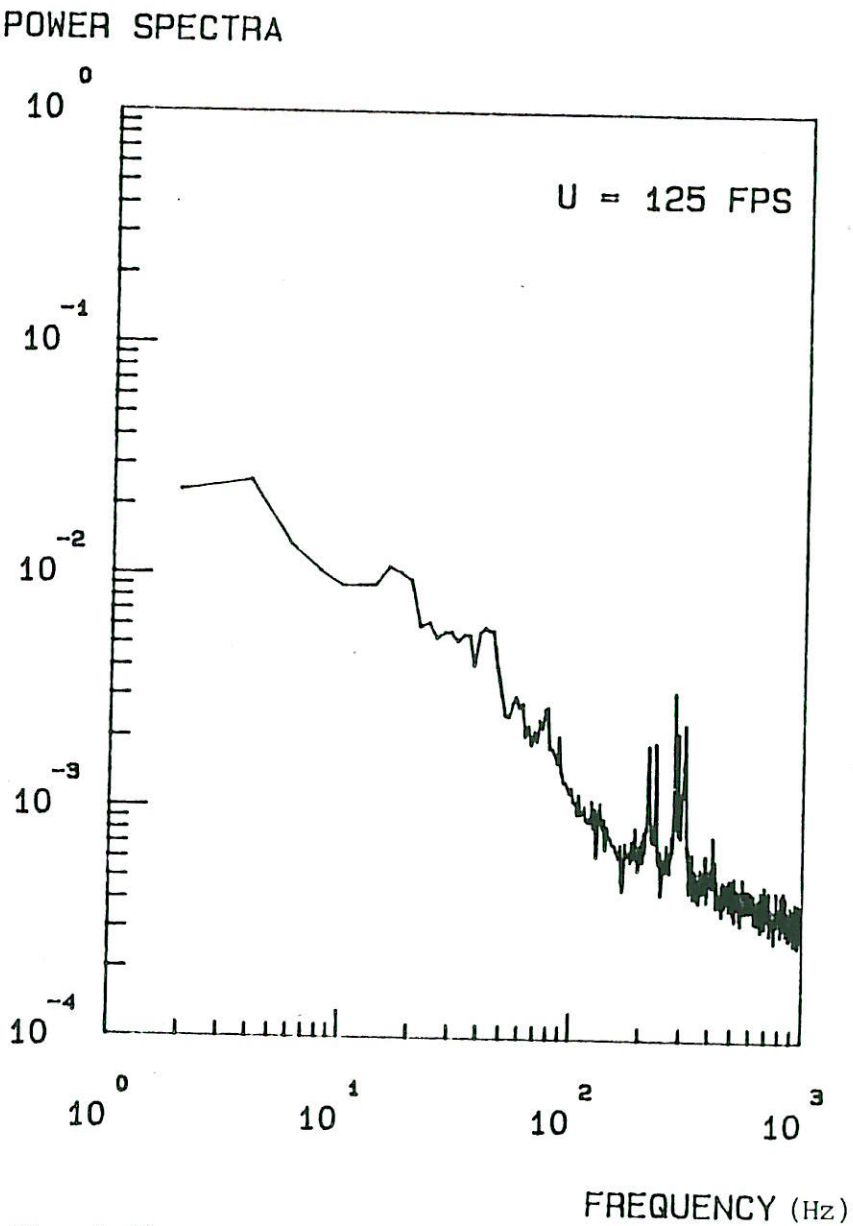

Fig. 7 i). Normalized power spectra at location C-3

$\overline{u^2}_{total}$=0.0229 fps^2, $\overline{u^2}_{turb}$=0.0162 fps^2

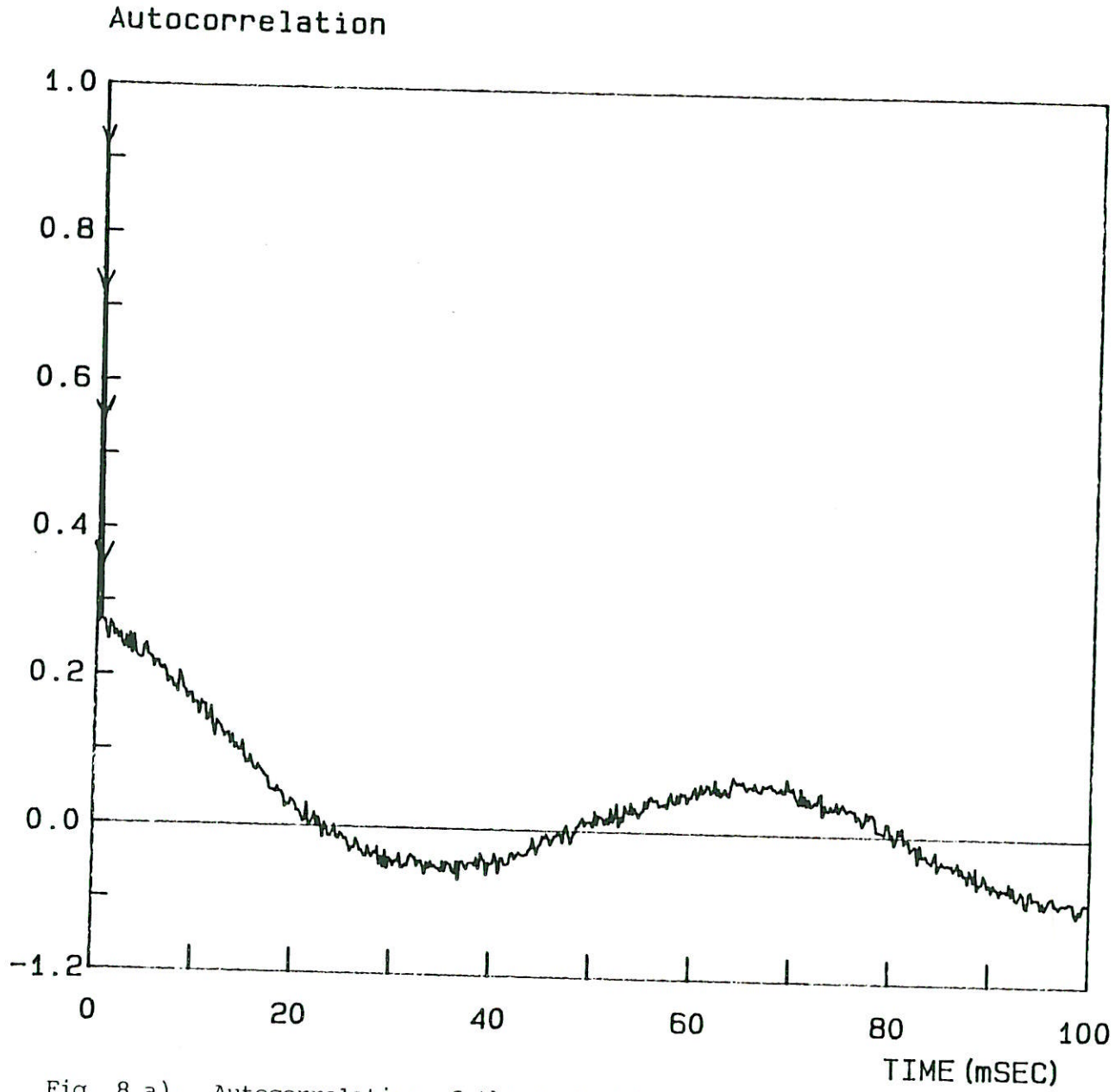

Fig. 8 a). Autocorrelation of the streamwise velocity fluctuation measured at the center of cross section (U = 50 fps).

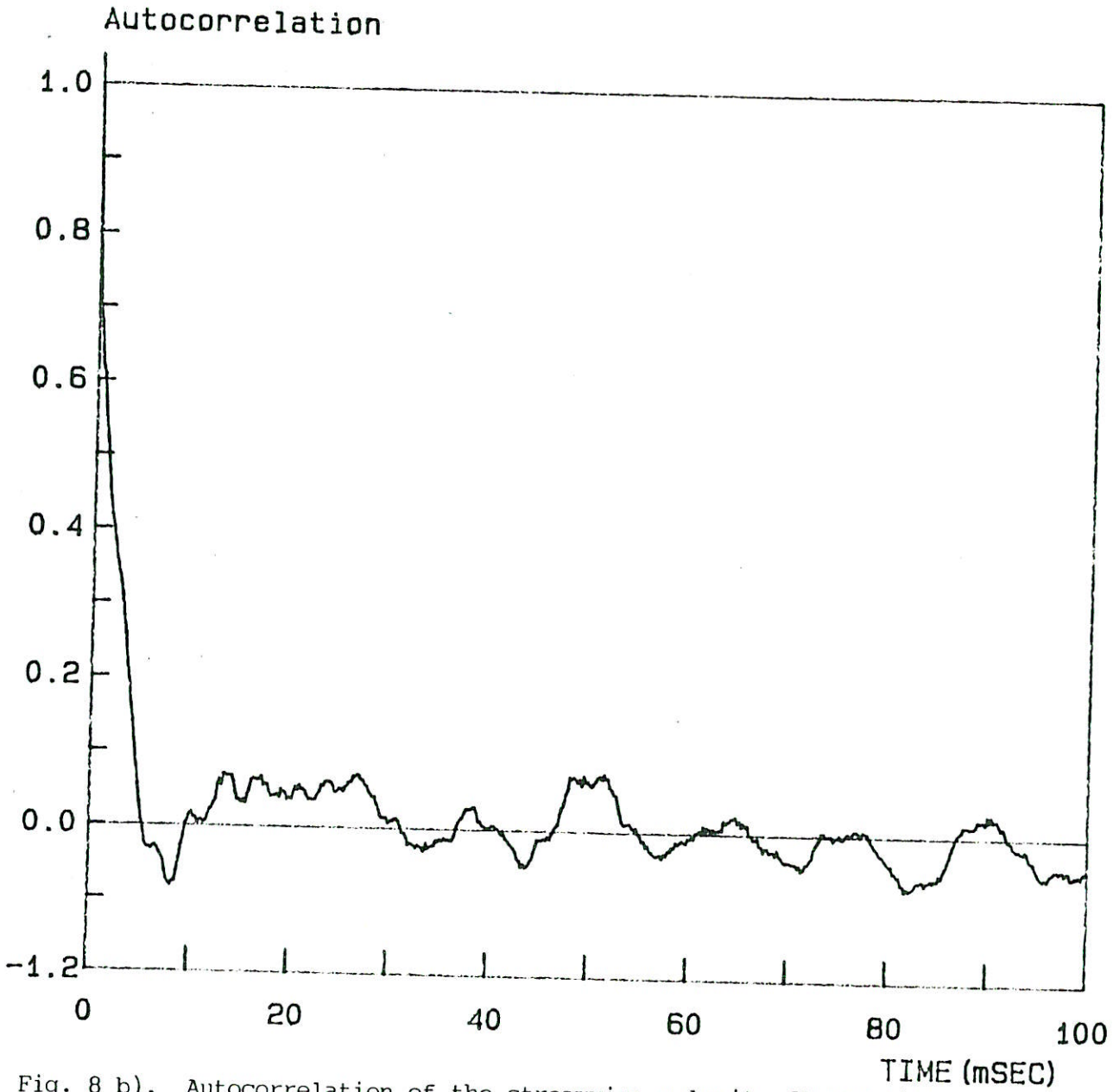

Fig. 8 b). Autocorrelation of the streamwise velocity fluctuation measured at the center of cross section (U = 125 fps).

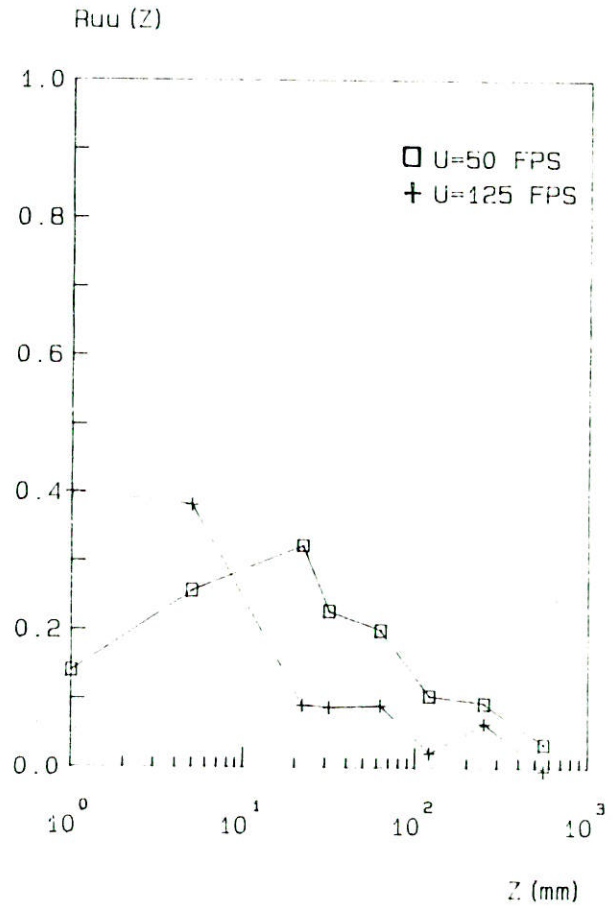

Fig. 9 (a). Space correlation of streamwise velocity fluctuation with spacings in z-direction.

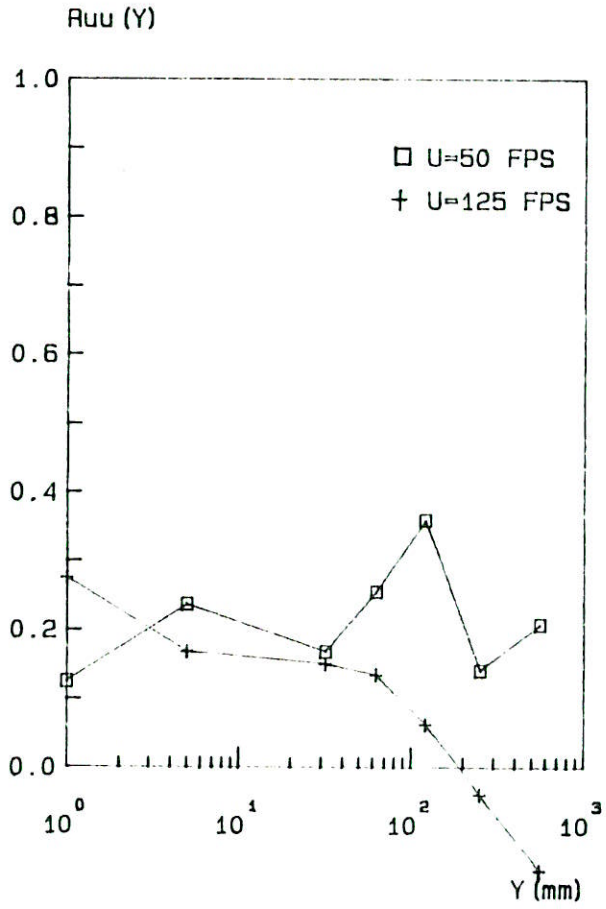

Fig. 9 (b). Space correlation of streamwise velocity fluctuation with spacings in y-direction.

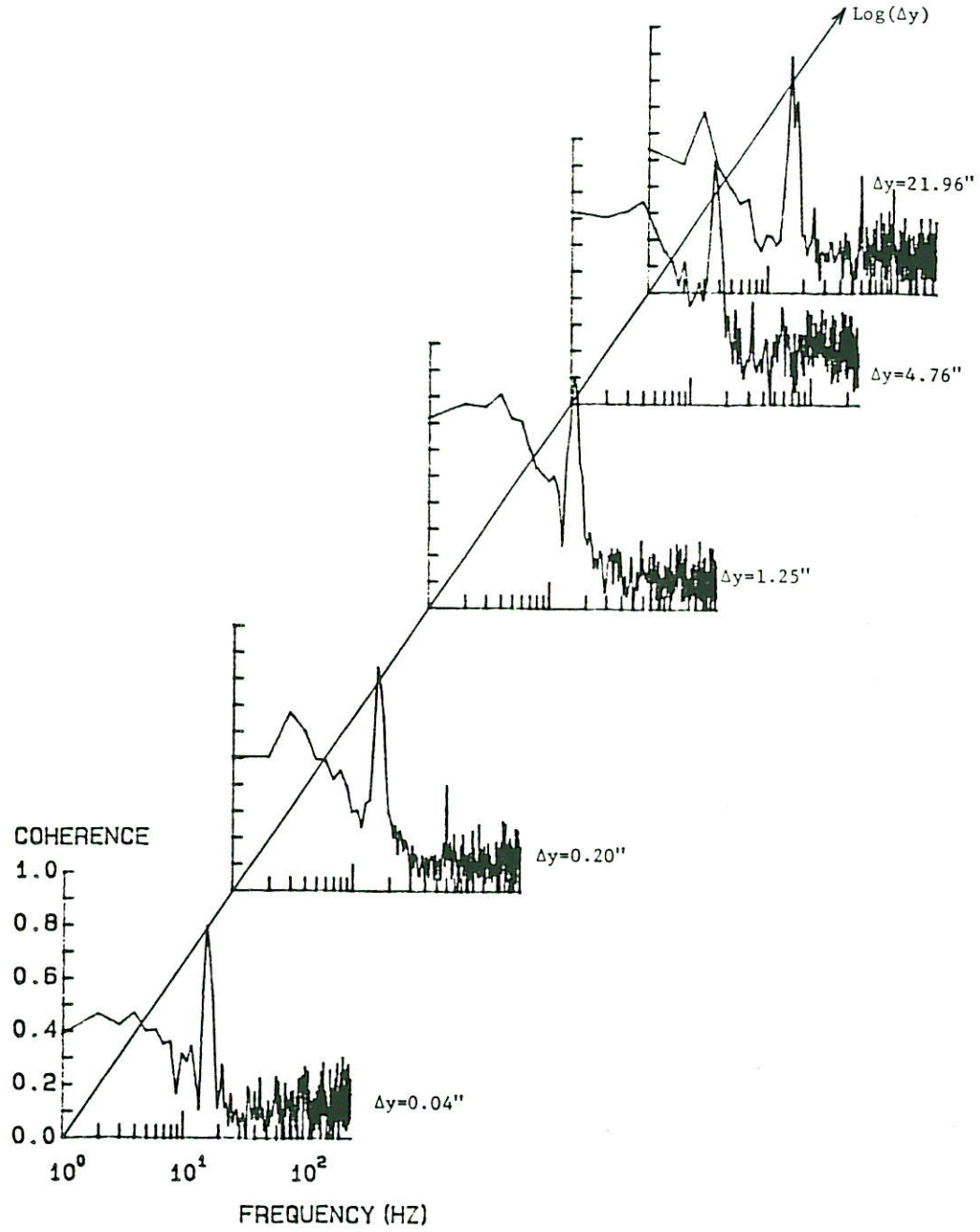

Fig. 10 a). Coherence with spacings in y-direction (U = 50 fps).

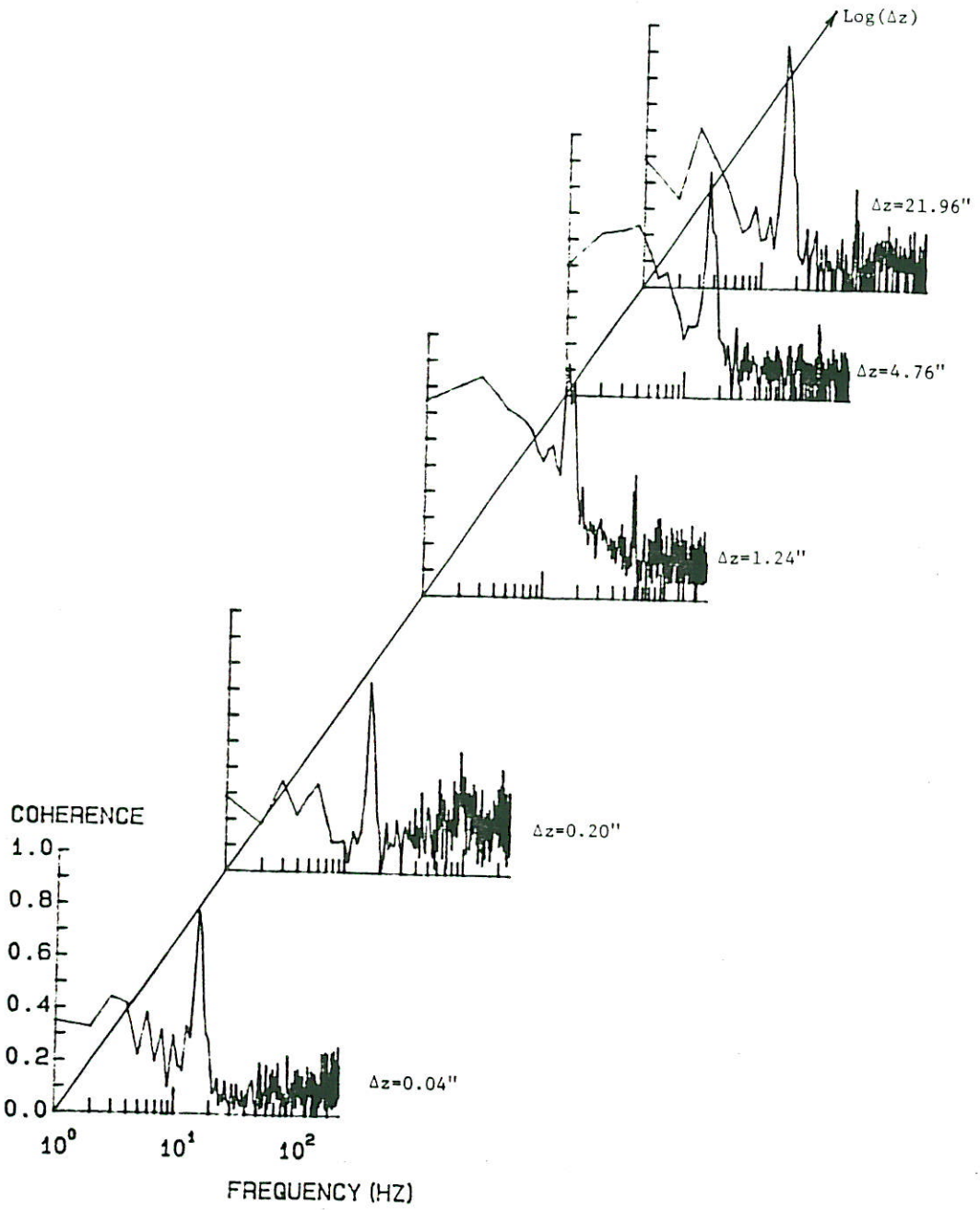

Fig. 10 b). Coherence with spacings in z-direction (U = 50 fps).

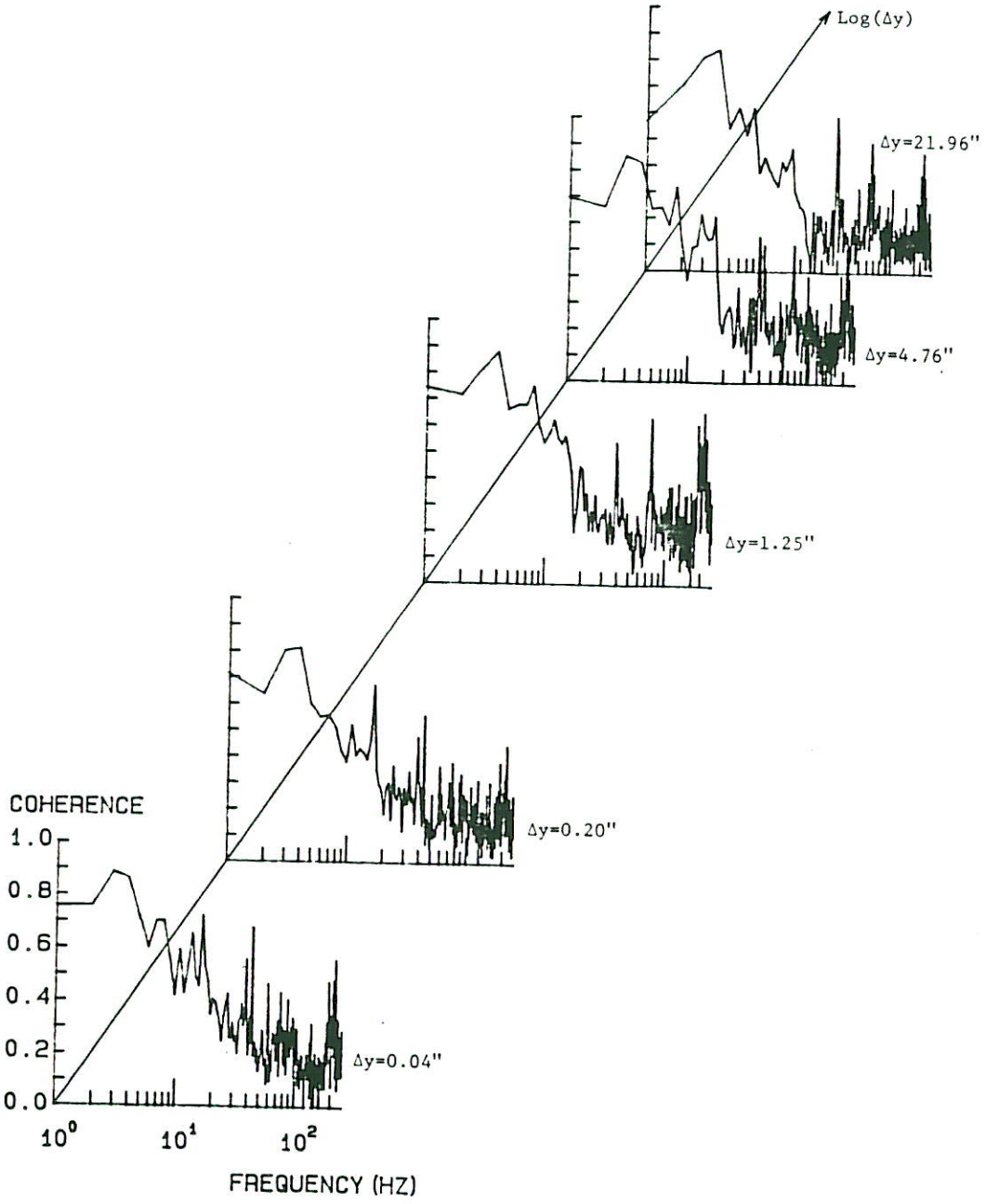

Fig. 10 c). Coherence with spacings in y-direction (U = 125 fps).

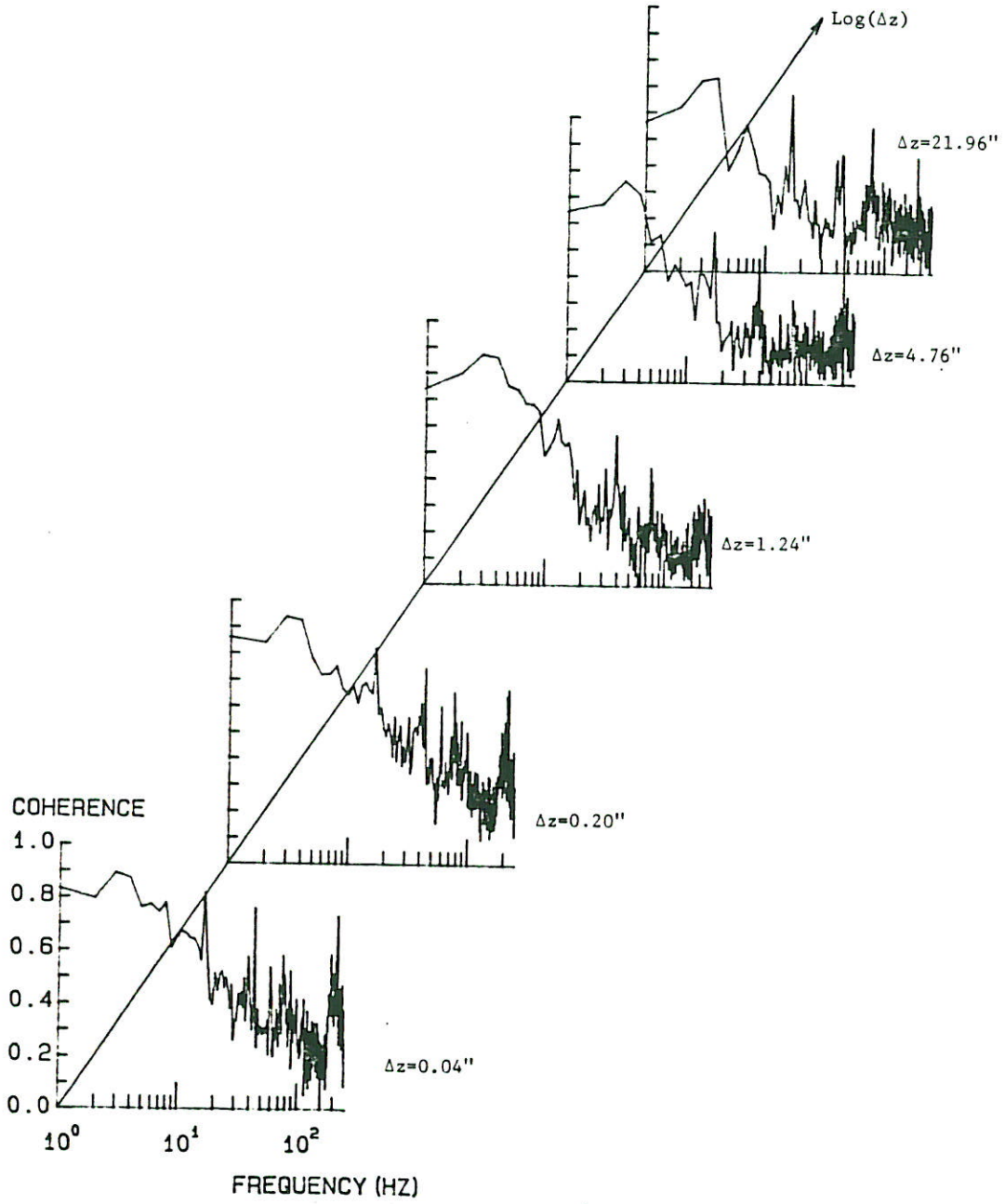

Fig. 10 d). Coherence with spacings in z-direction (U = 125 fps).

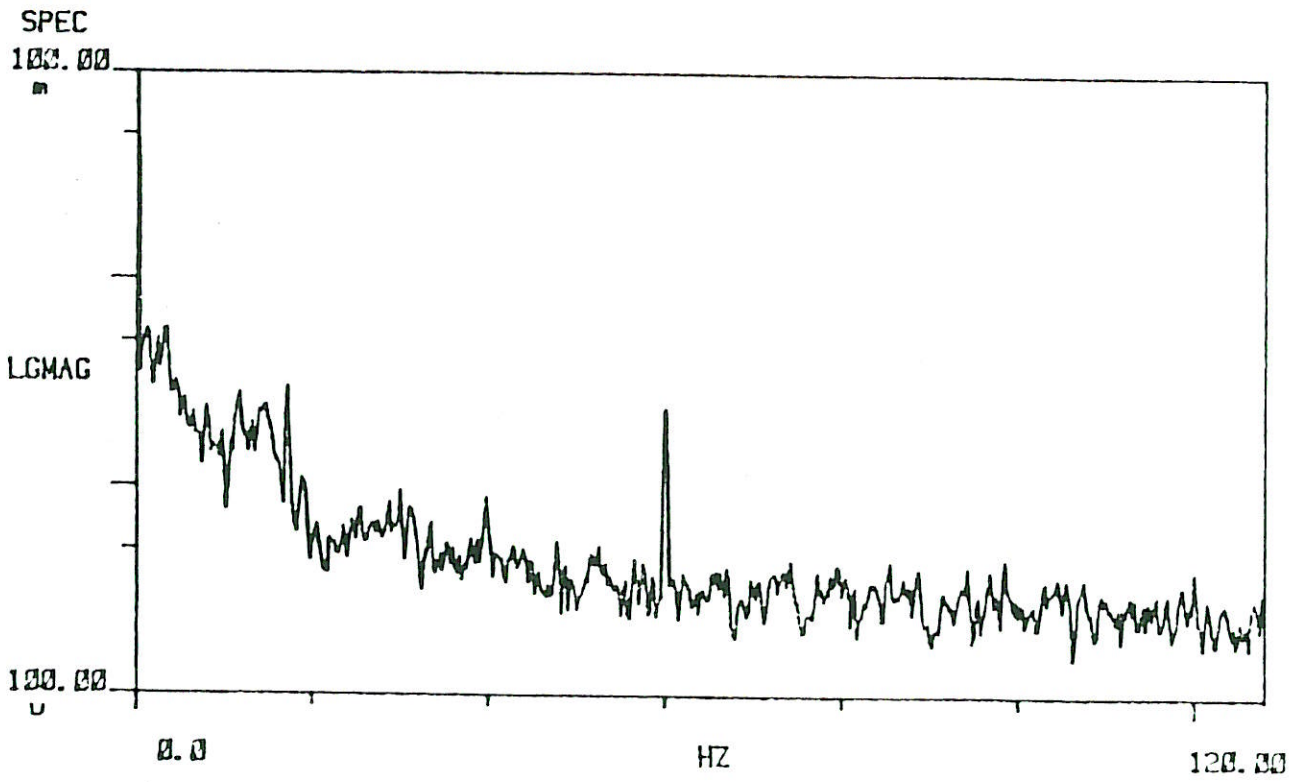

Fig. 2 b). Turbulence spectrum at U = 49.2 fps (Reynolds, 1982)

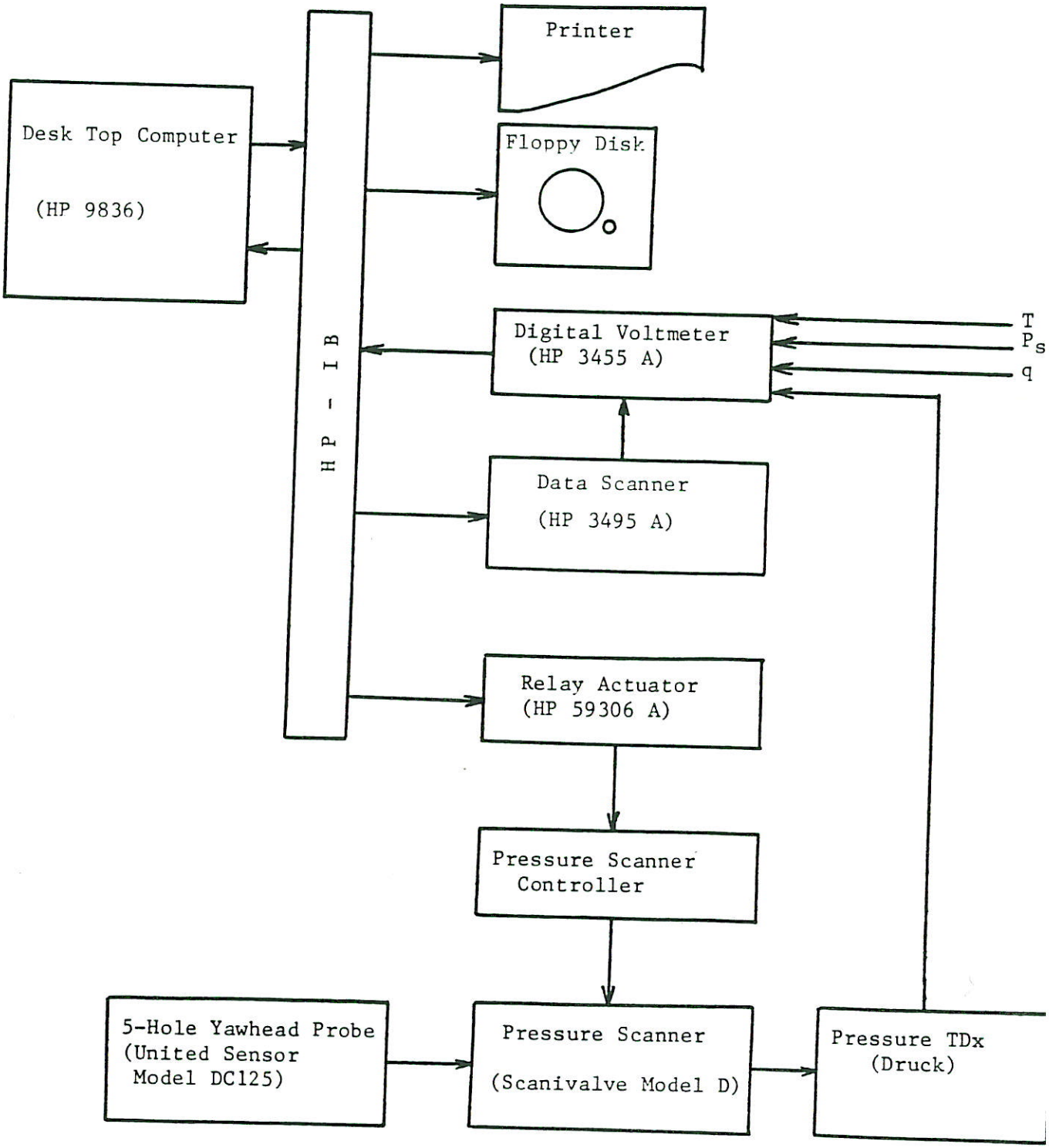

Fig. 3 a). Schematic diagram of instrumentation (for measurements with yawhead probe)

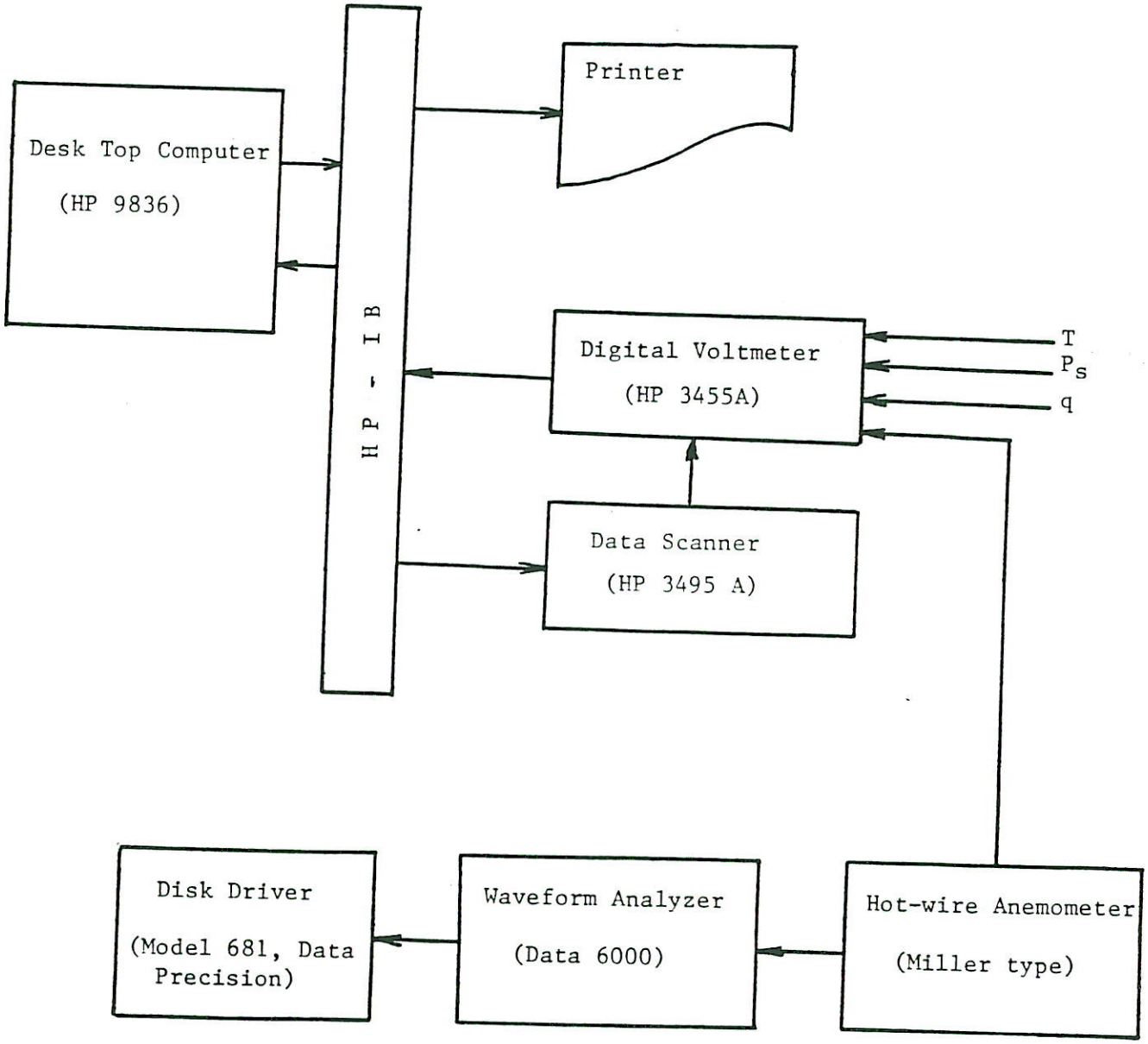

Fig. 3 b). Schematic diagram of instrumentation (for measurements with hot-wire).

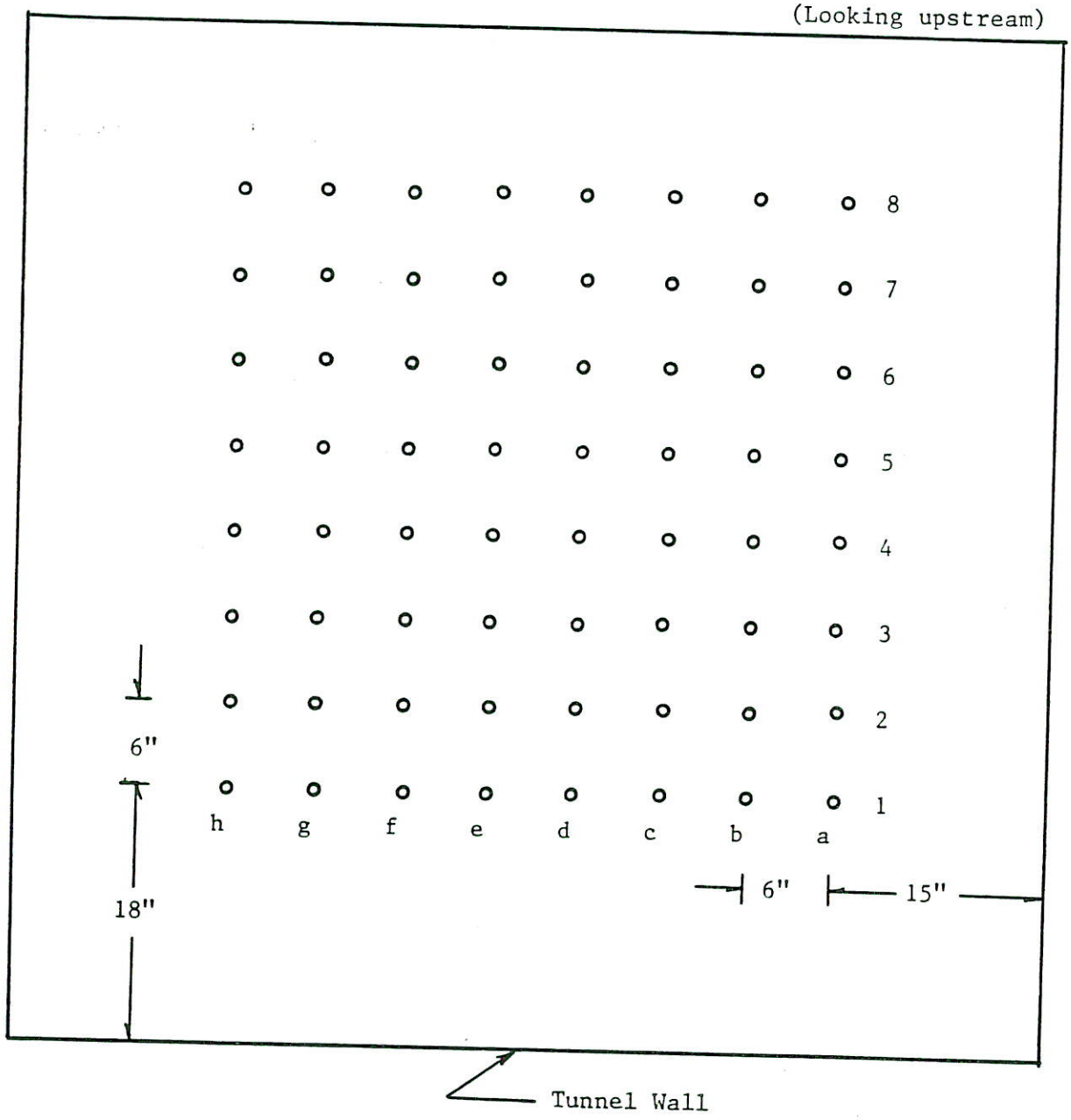

Fig. 4 a). Location of probe (for measurements with yawhead probe).

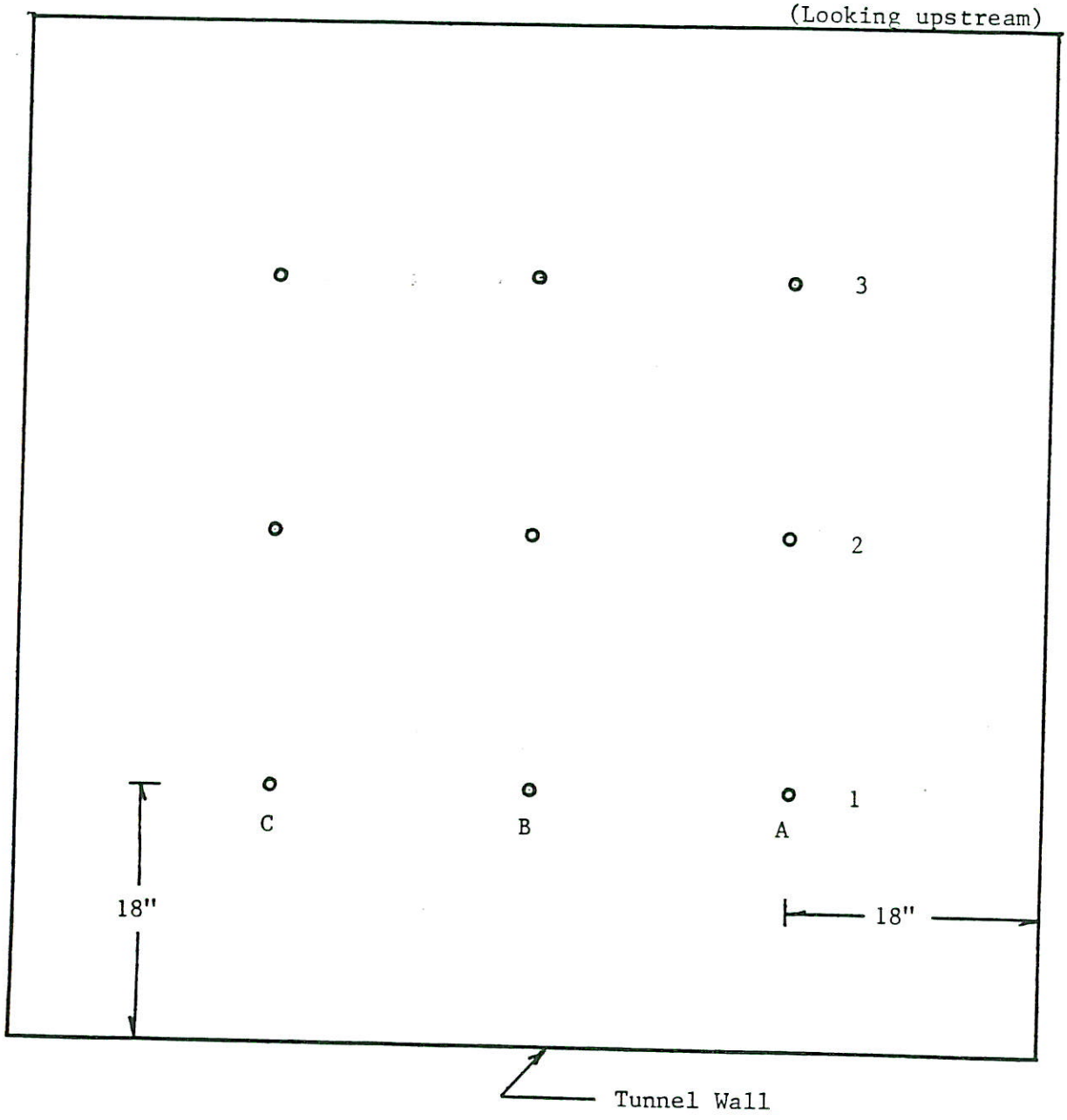

Fig. 4 b). Location of probe (for measurements with hot-wire probe).

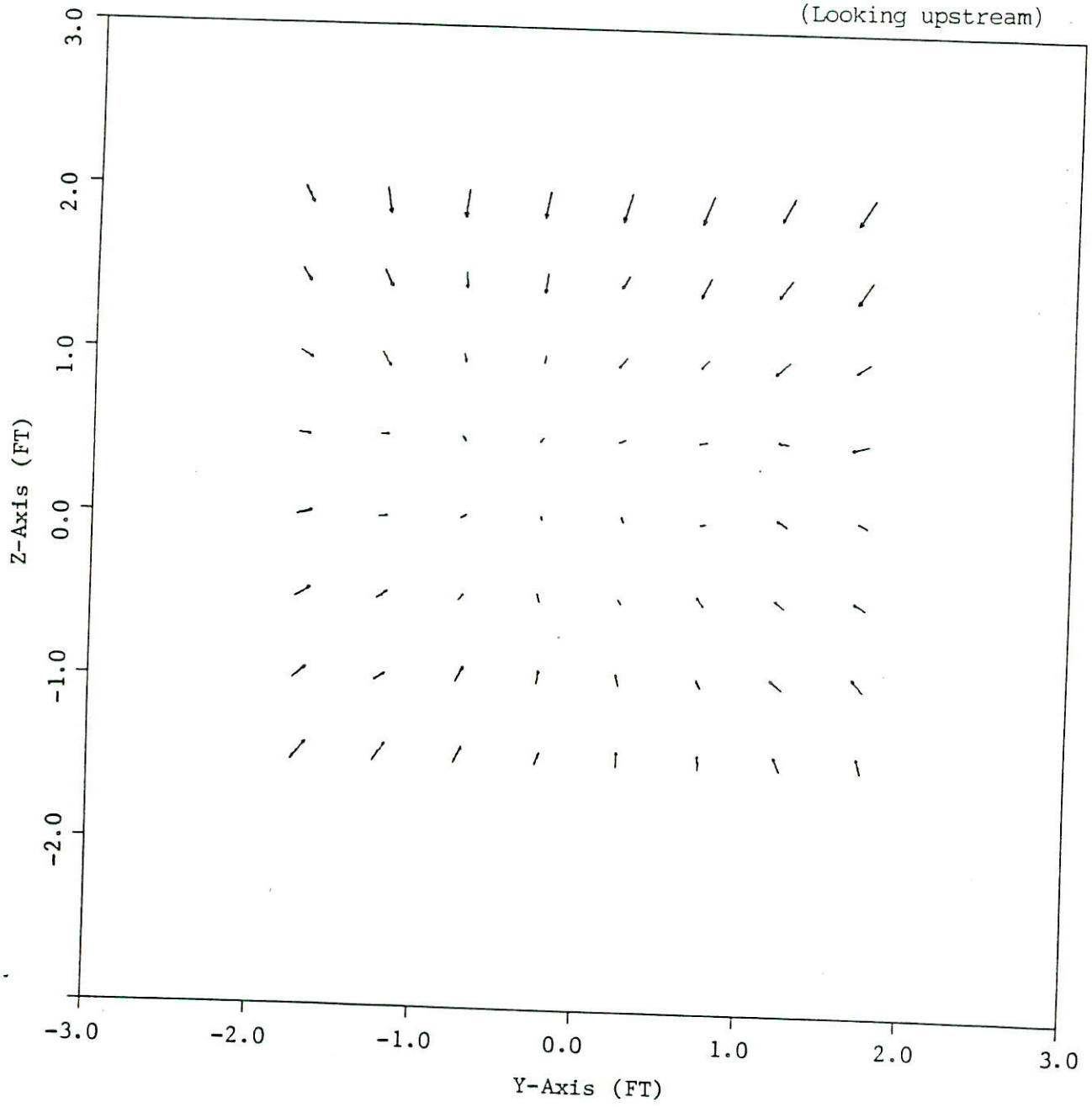

FIG. 5 a) Velocity vector across the test section at U = 50 fps (1 inch = 10 fps).

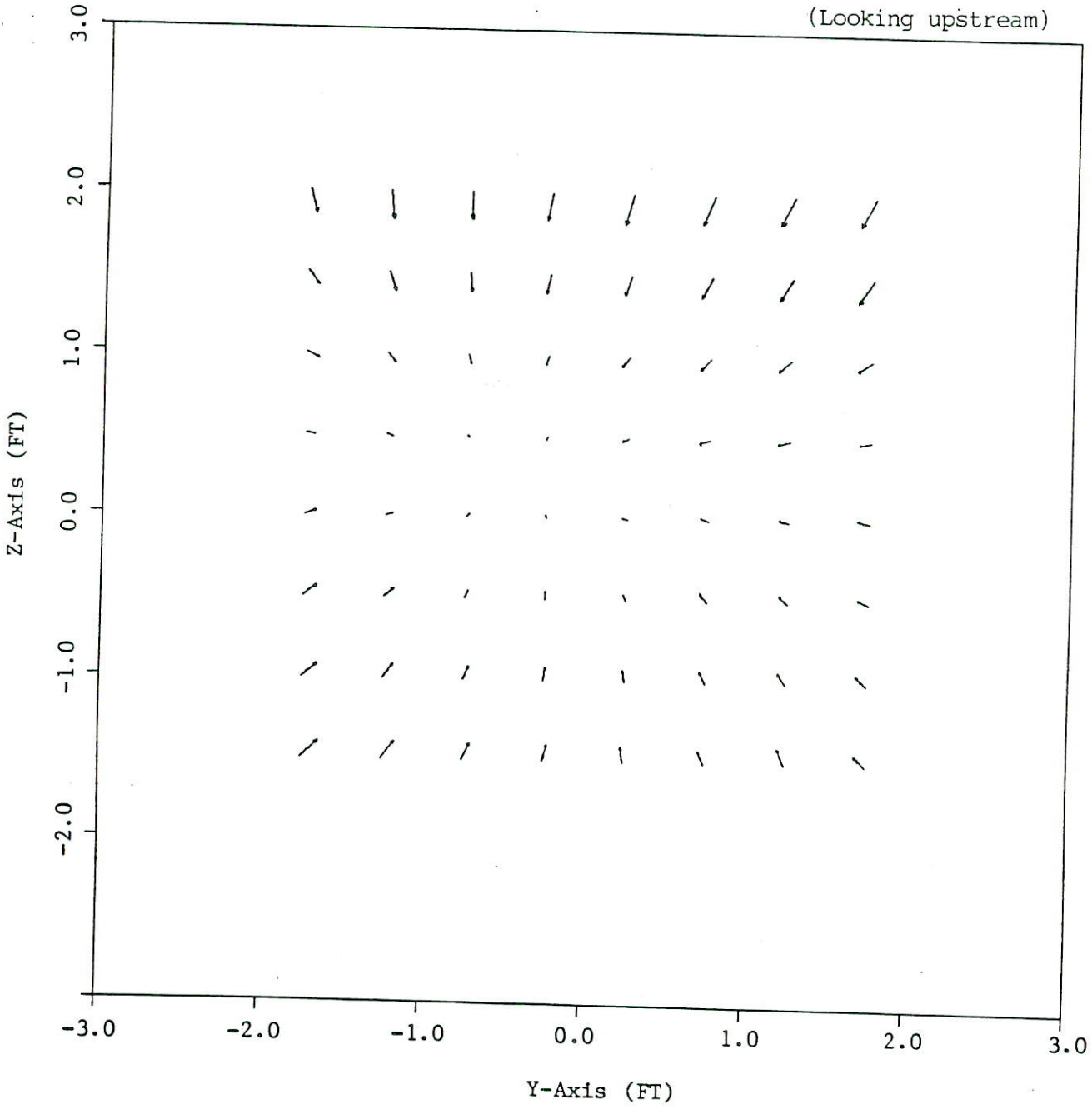

Fig. 5 b). Velocity vector across the test section at U = 125 fps (1 inch = 25 fps).

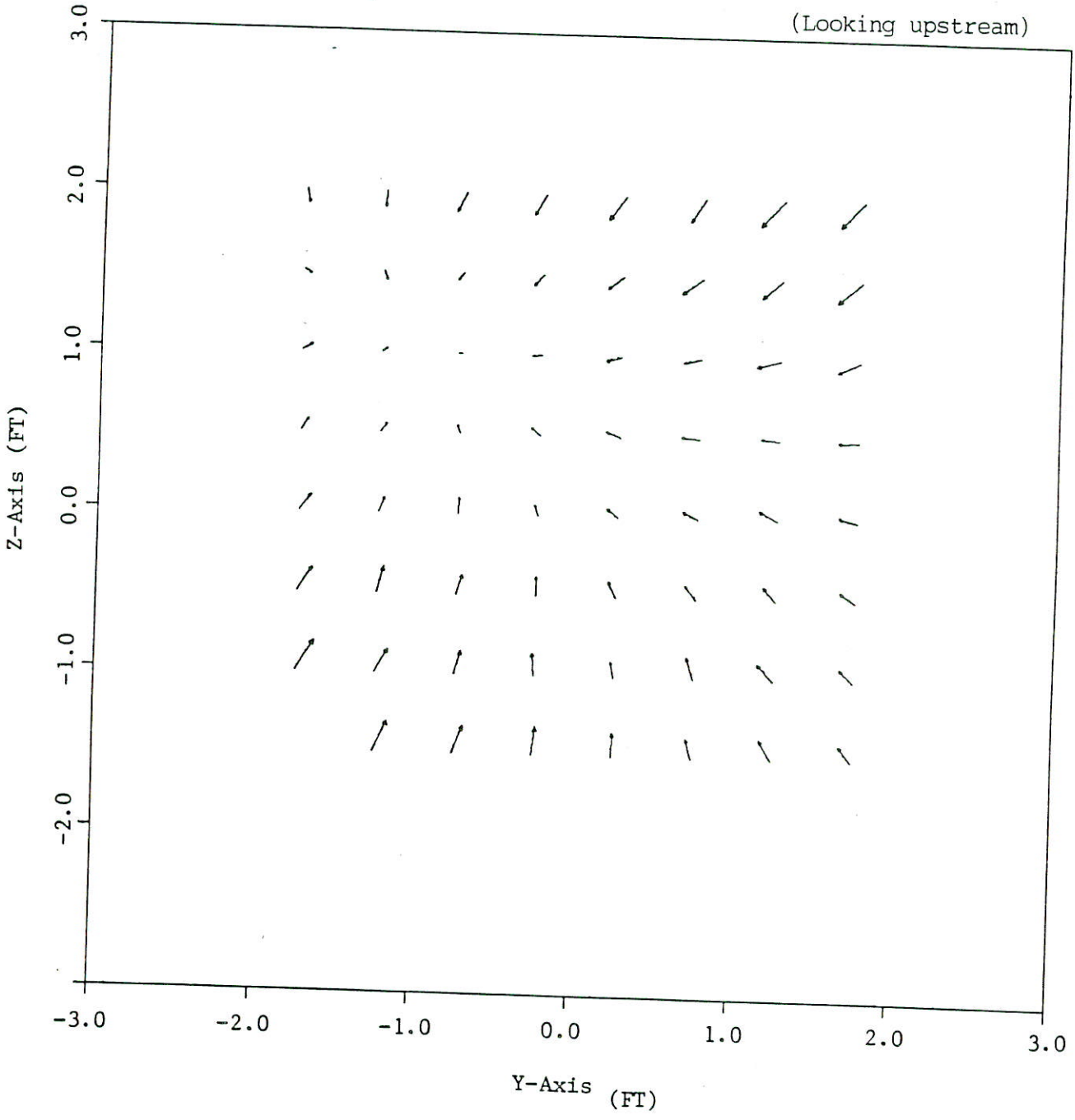

Fig. 5 c). Velocity vector across the test section at U = 200 fps (1 inch = 40 fps).

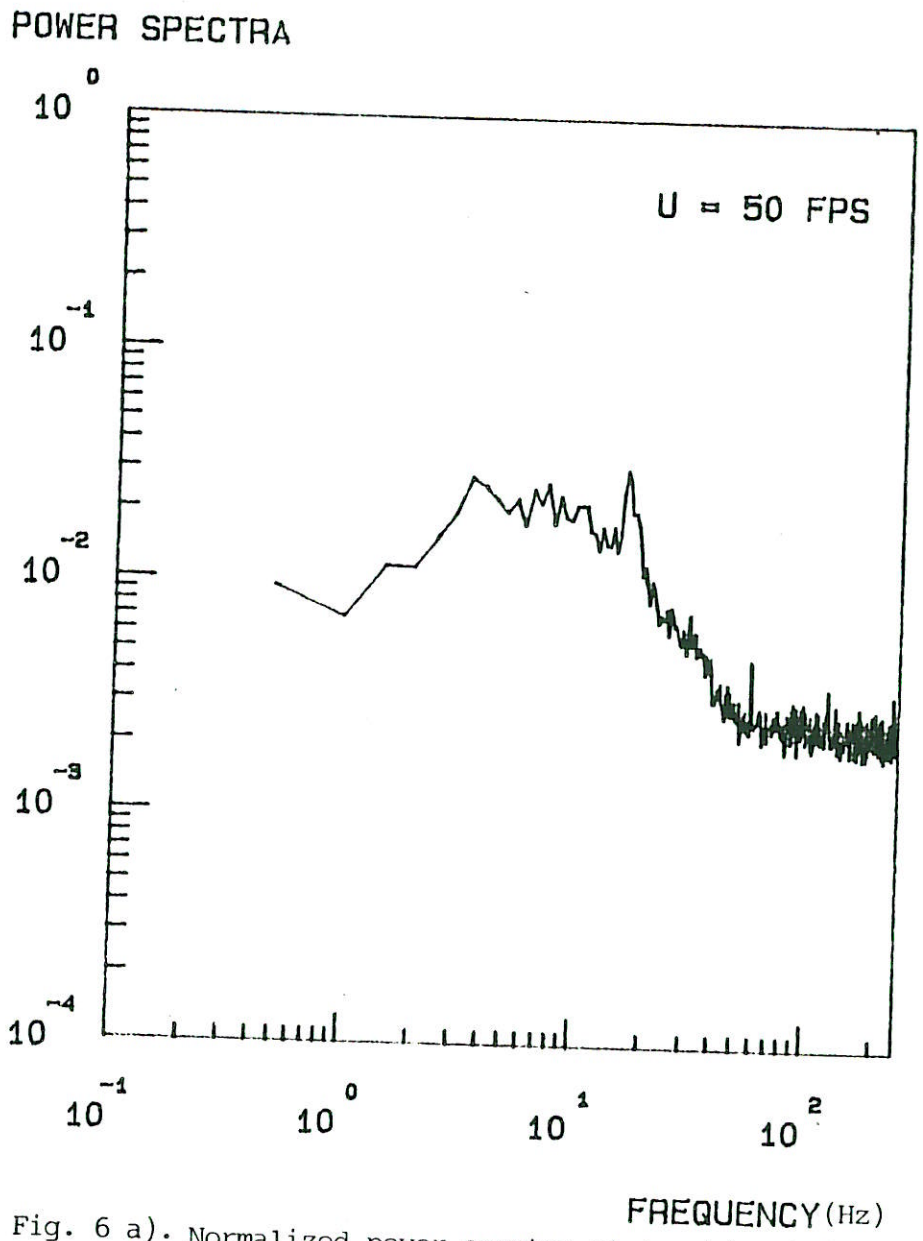

Fig. 6 a). Normalized power spectra at location A-1

$\overline{u^2}_{total}$=0.0011 fps^2, $\overline{u^2}_{turb}$=0.0007 fps^2

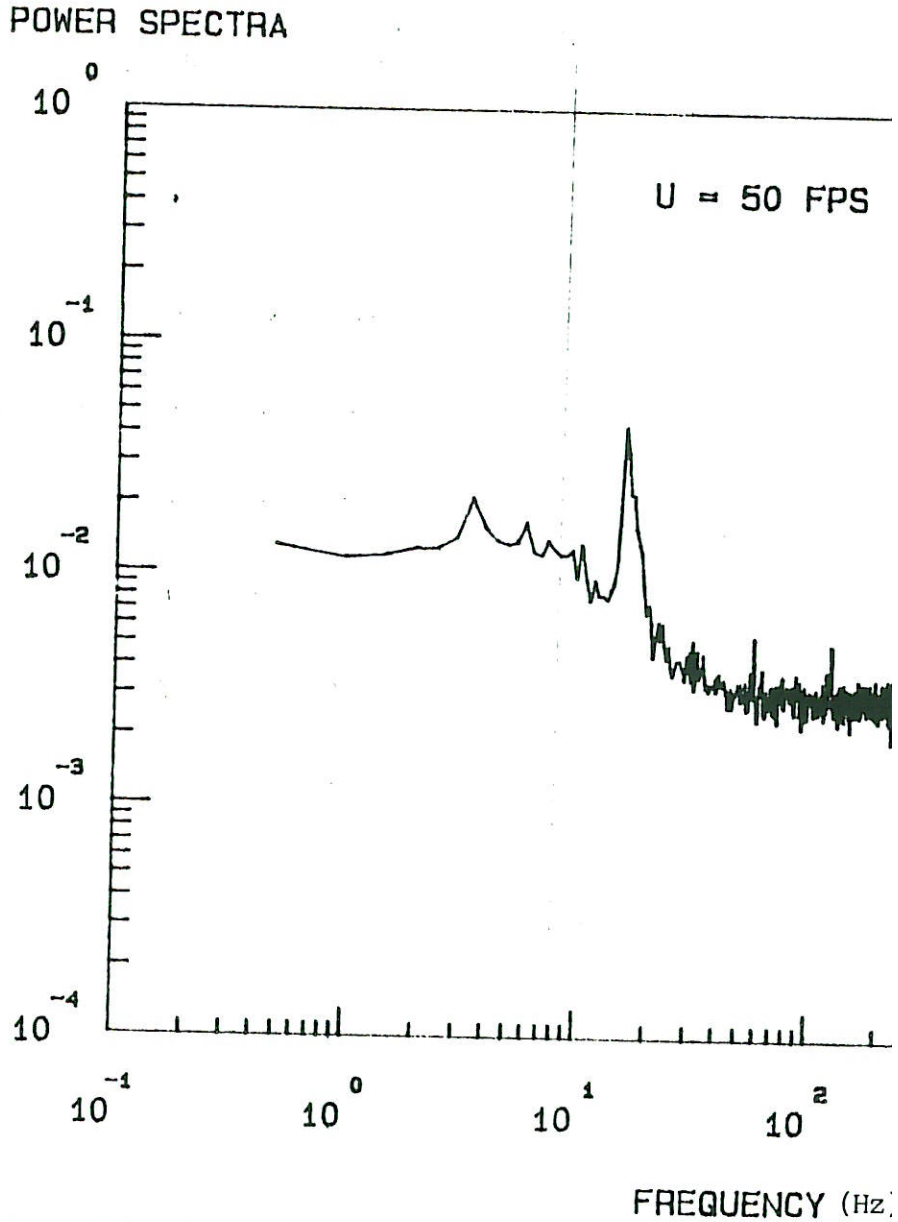

Fig. 6 b). Normalized power spectra at location A-2

$\overline{u^2}$ =0.0008 fps^2, $\overline{u^2}$ =0.0005 fps^2

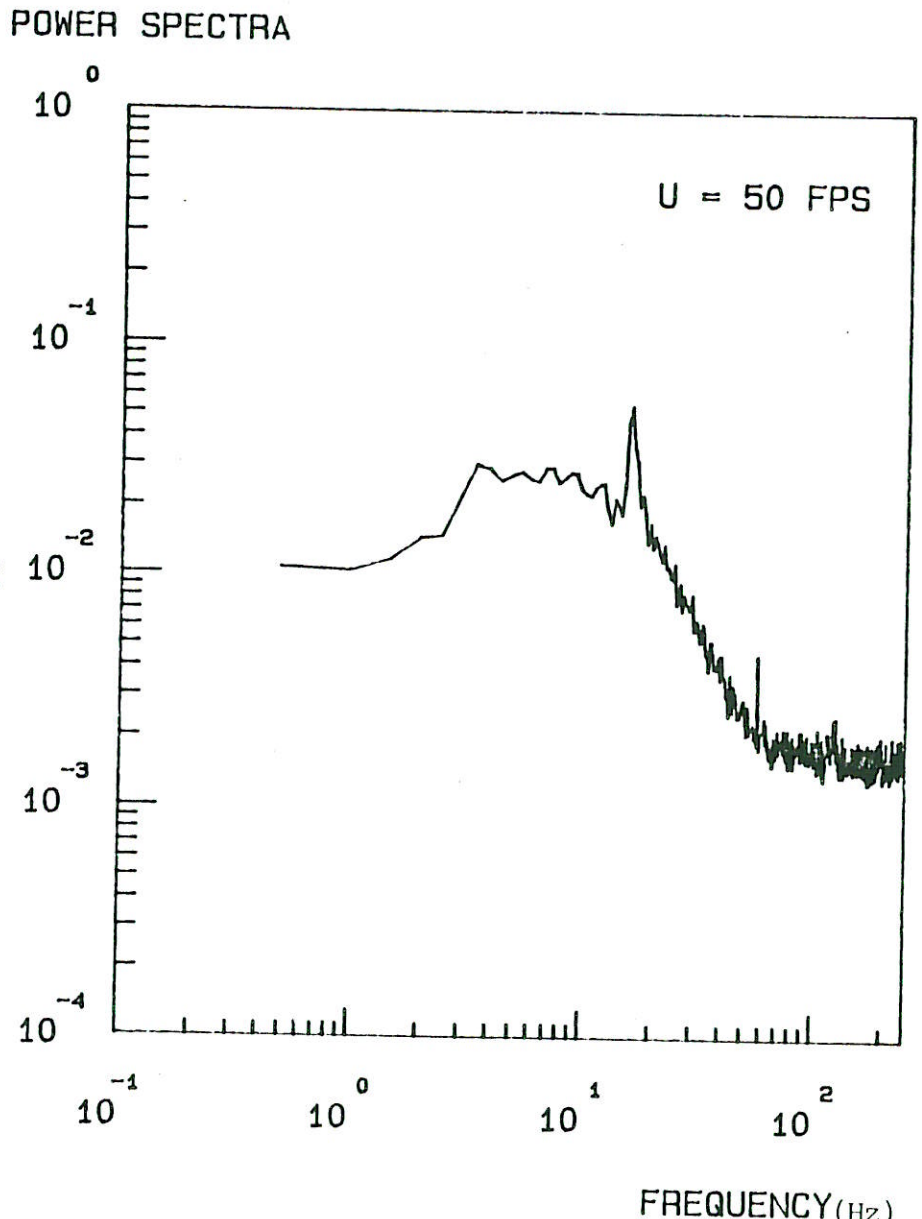

Fig. 6 c). Normalized power spectra at location A-3

$\overline{u^2}_{total}$=0.0010 fps^2, $\overline{u^2}_{turb}$=0.0007 fps^2

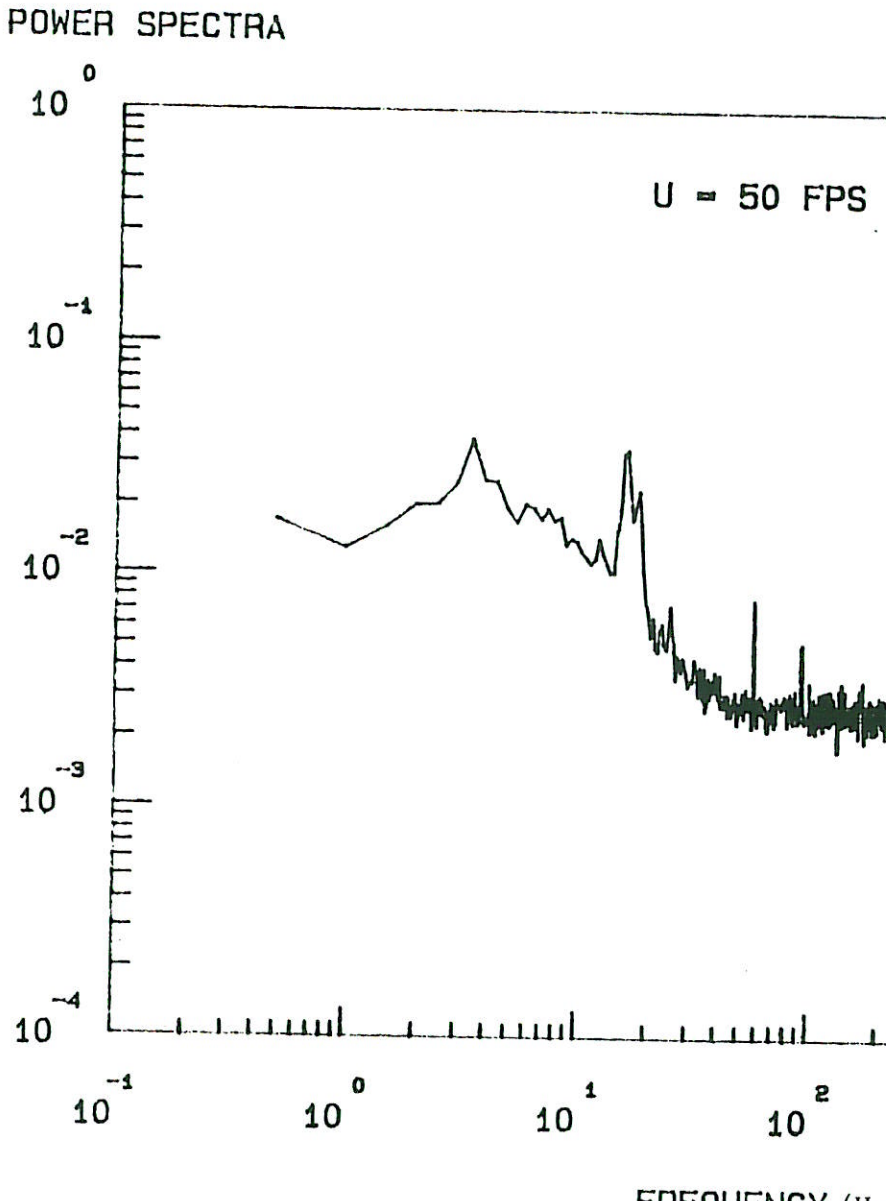

Fig. 6 d). Normalized power spectra at location B-1

$\overline{u^2}_{total}$=0.0006 fps^2, $\overline{u^2}_{turb}$=0.0003 fps^2

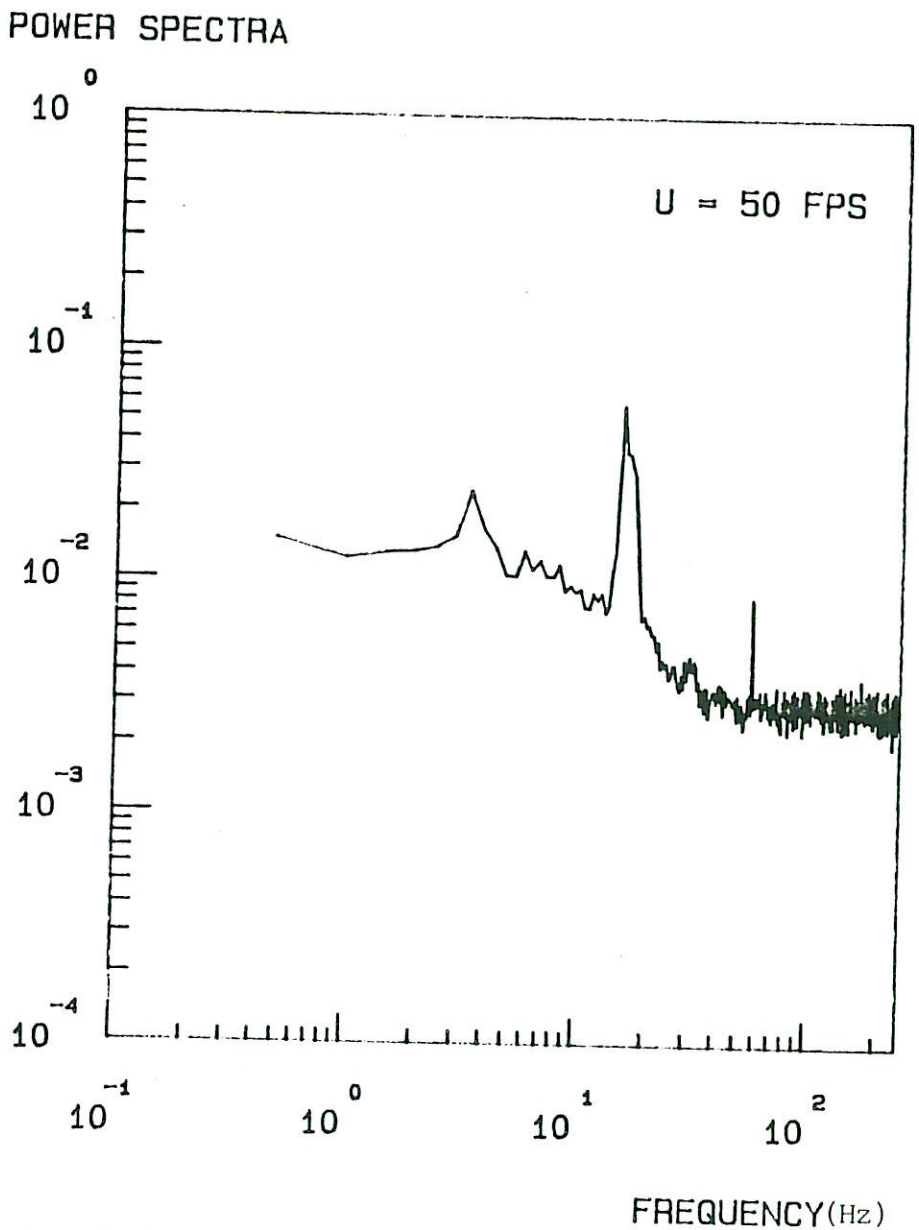

Fig. 6 e). Normalized power spectra at location B-2

$\overline{u^2}_{total}$=0.0006 fps^2, $\overline{u^2}_{turb}$=0.0004 fps^2

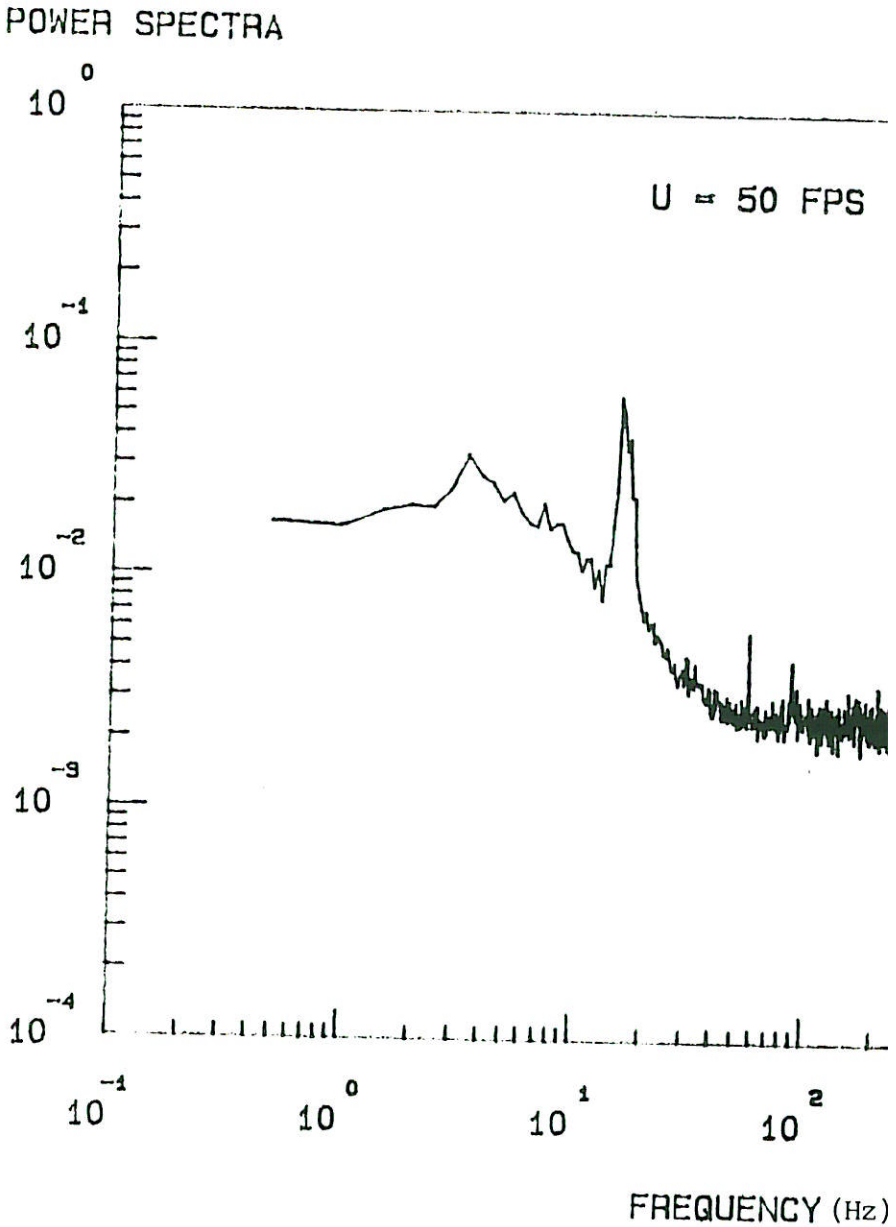

Fig. 6 f). Normalized power spectra at location B-3

$\overline{u^2}_{total}$=0.0007 fpa^2, $\overline{u^2}_{turb}$=0.0004 fps^2

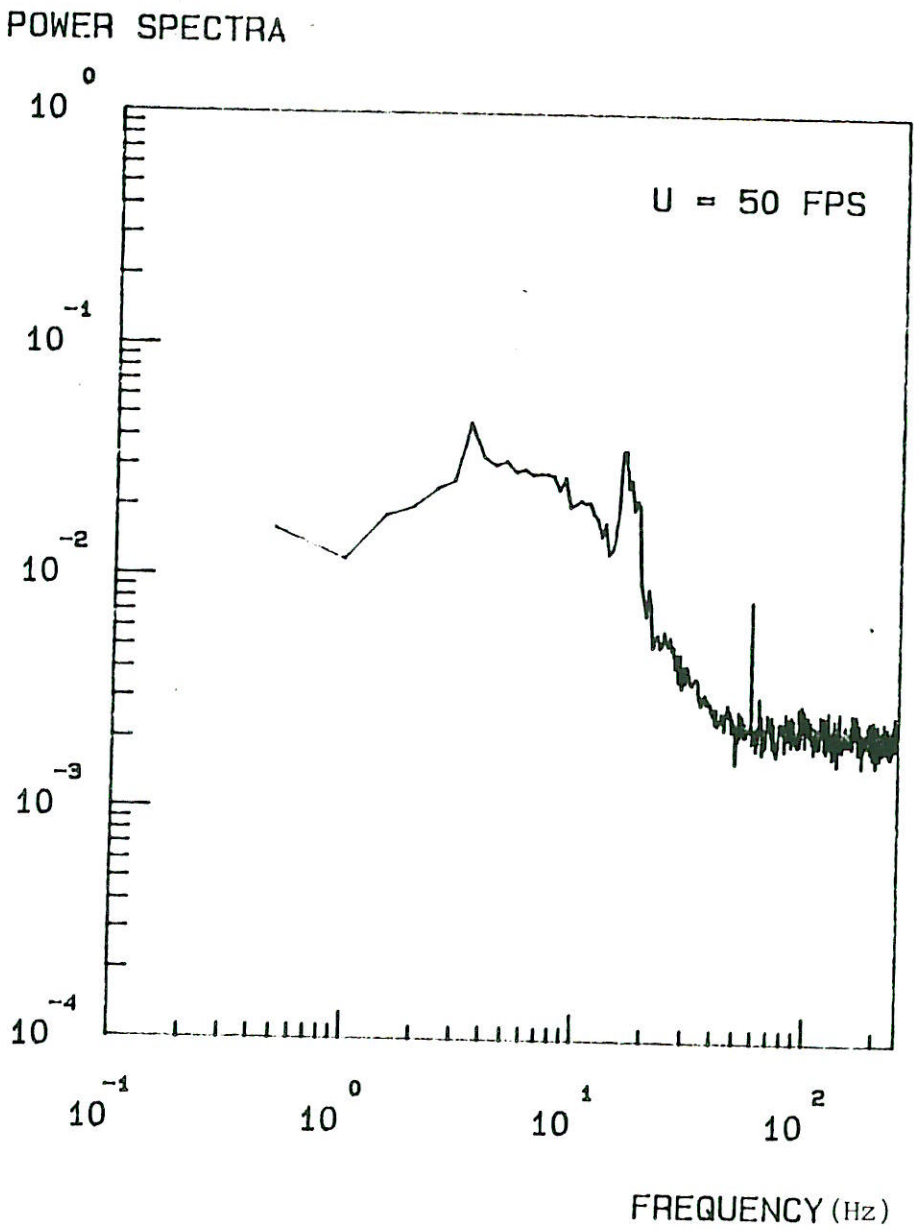

Fig. 6 g). Normalized power spectra at location C-1

$\overline{u^2}_{total}$=0.0007 fps^2, $\overline{u^2}_{turb}$=0.0004 fps^2

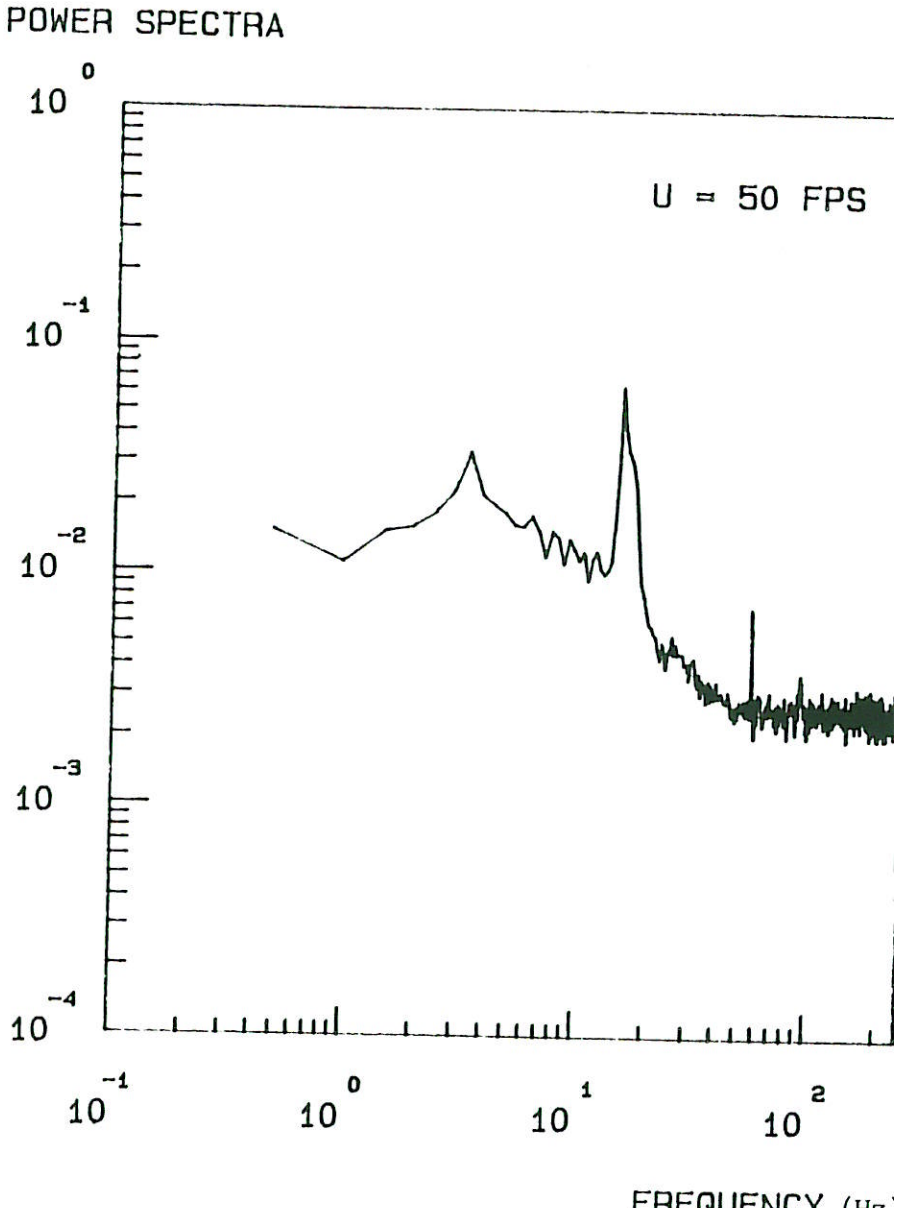

Fig. 6 h). Normalized power spectra at location C-2

$\overline{u^2}_{total}$=0.0006 fps, $\overline{u^2}$, =0.0004 fps^2

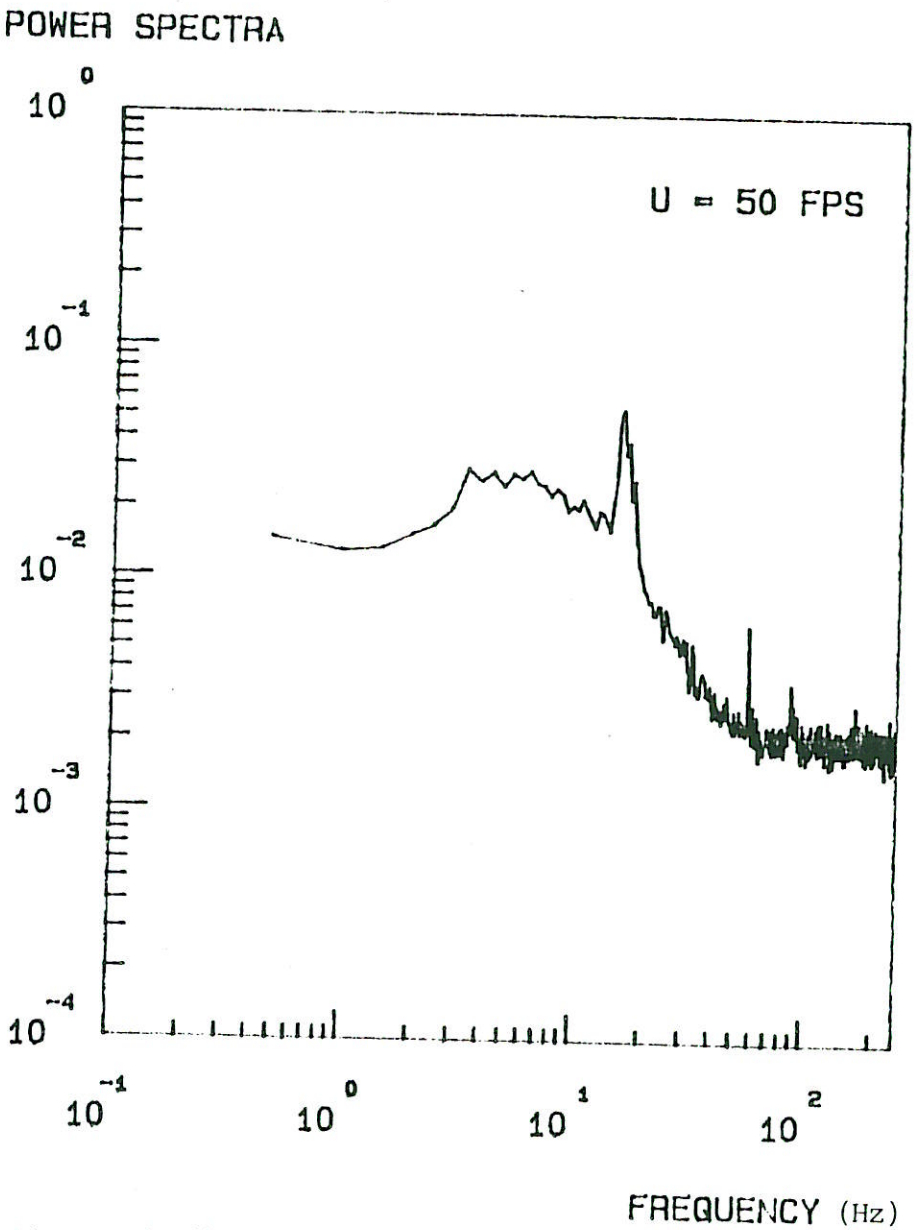

Fig. 6 i). Normalized power spectra at location C-3

$\overline{u^2}_{total}$=0.0008 fps^2, $\overline{u^2}_{turb}$=0.0005 fps^2

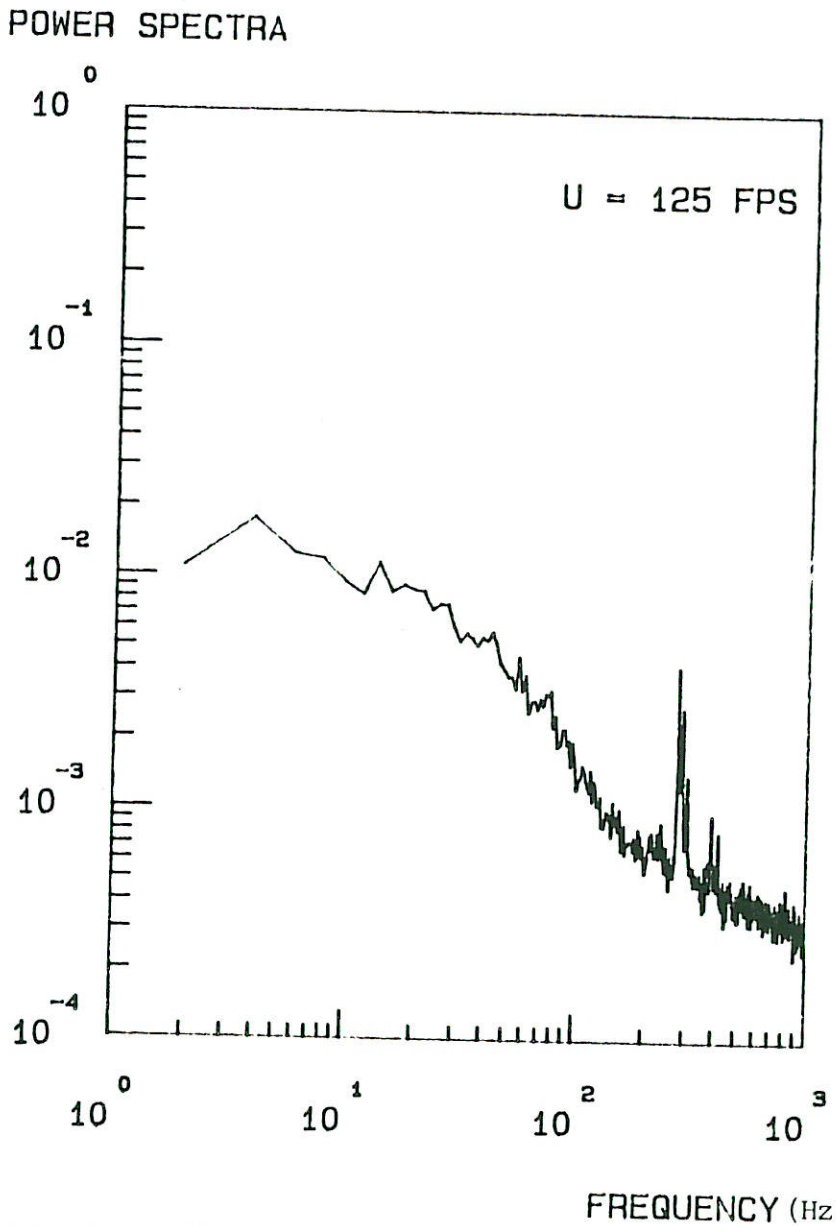

Fig. 7 a). Normalized power spectra at location A-1

$\overline{u^2}_{total}$=0.0315 fps^2, $\overline{u^2}_{turb}$=0.0229 fps^2

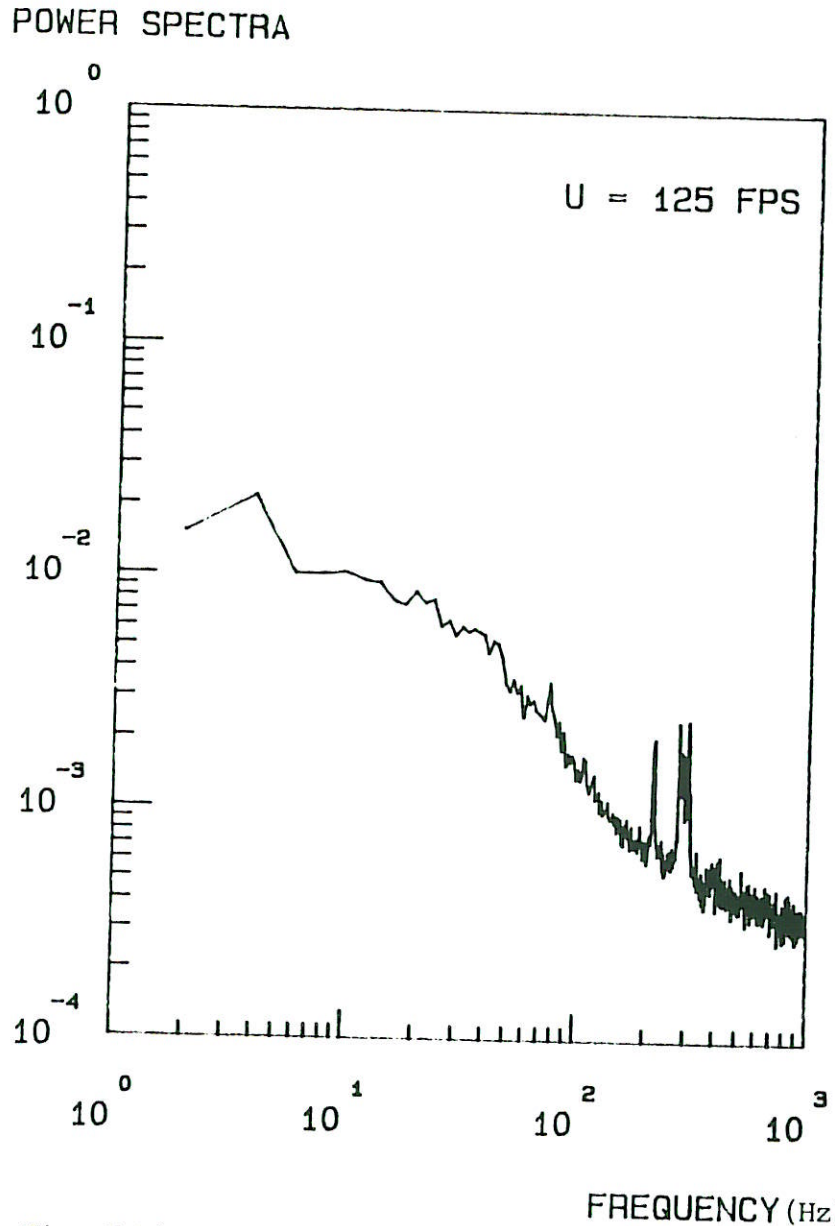

Fig. 7 b). Normalized power spectra at location A-2

$\overline{u^2}_{total}$=0.0283 fps^2, $\overline{u^2}_{turb}$=0.0208 fps^2

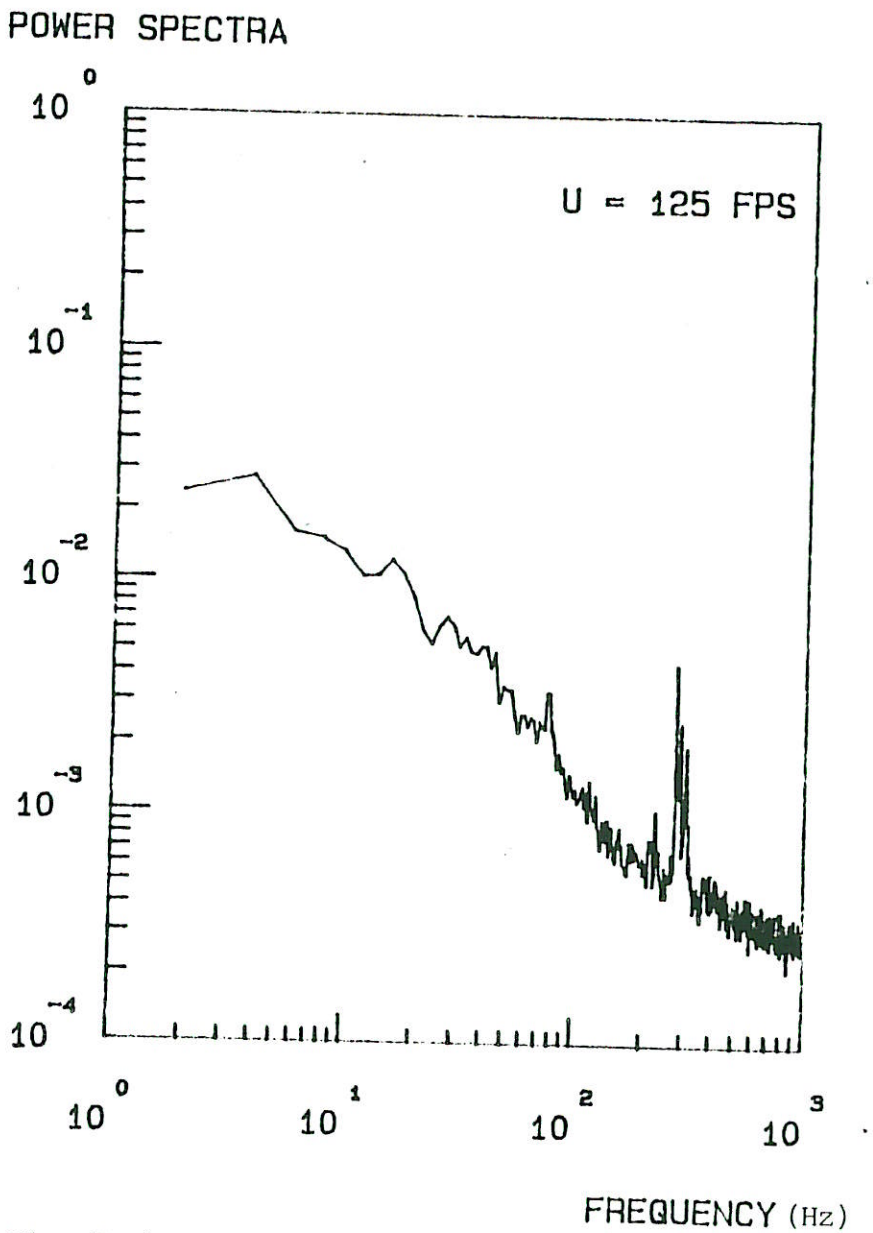

Fig. 7 c) Normalized power spectra at location A-3

$\overline{u^2}_{total}$=0.0247 fps^2, $\overline{u^2}_{turb}$=0.0178 fps^2

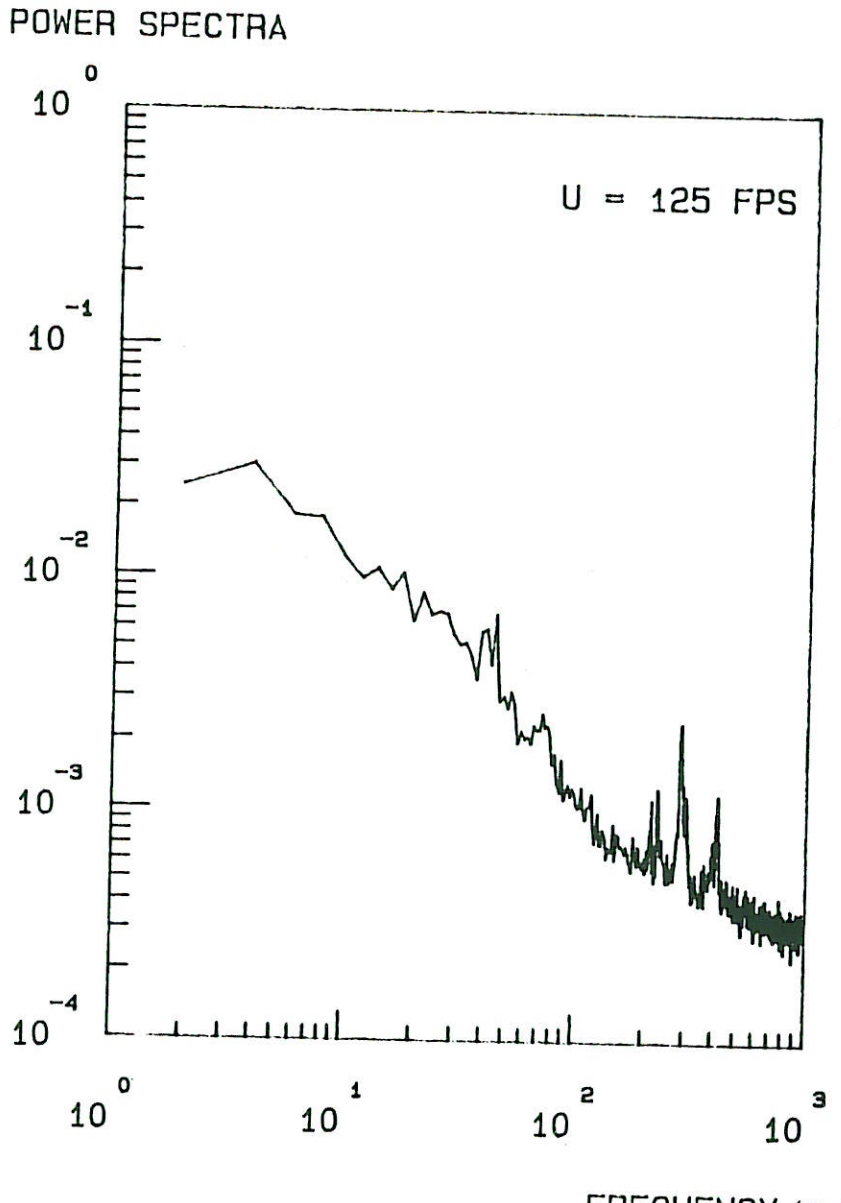

Fig. 7 d). Normalized power spectra at location B-1

$\overline{u^2}_{total}$=0.0211 fps^2, $\overline{u^2}_{turb}$=0.0152 fps^2

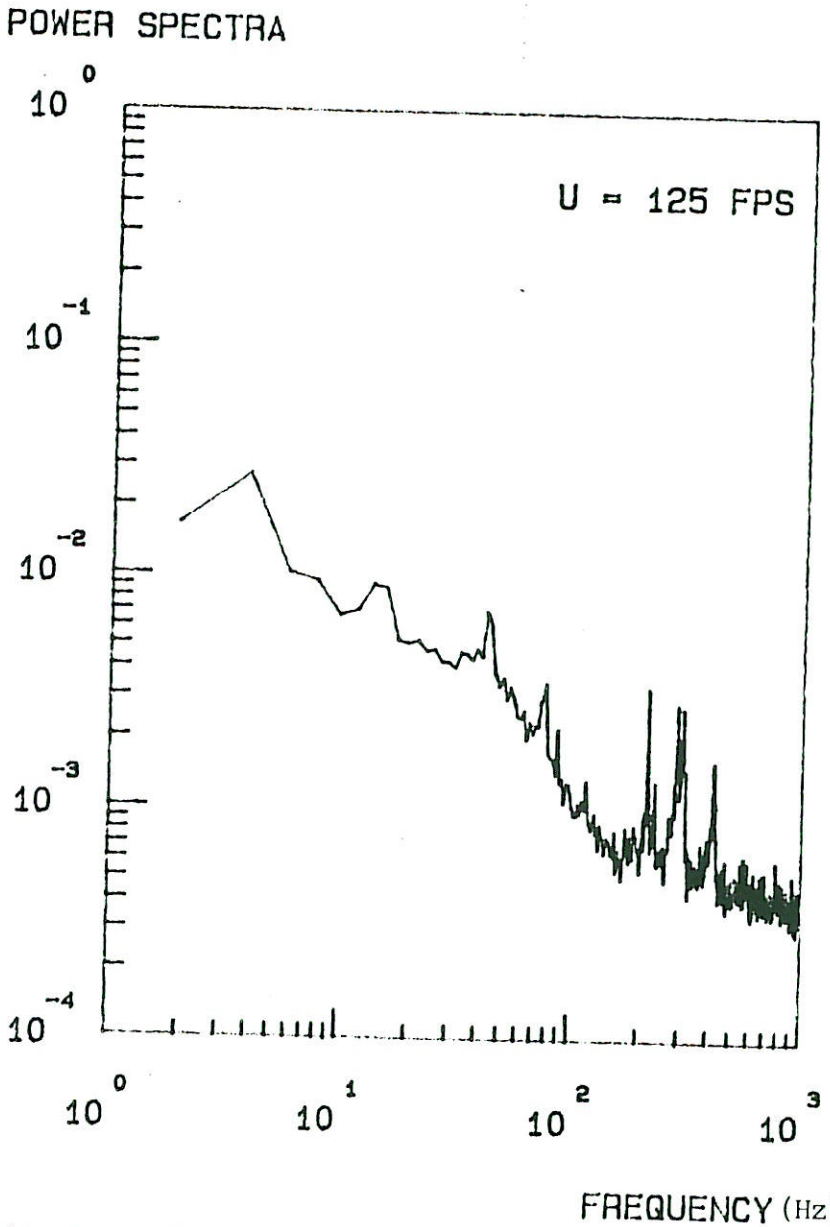

Fig. 7 e). Normalized power spectra at location B-2

$\overline{u^2}_{total}$=0.0147 fps^2, $\overline{u^2}_{turb}$=0.0081 fps^2

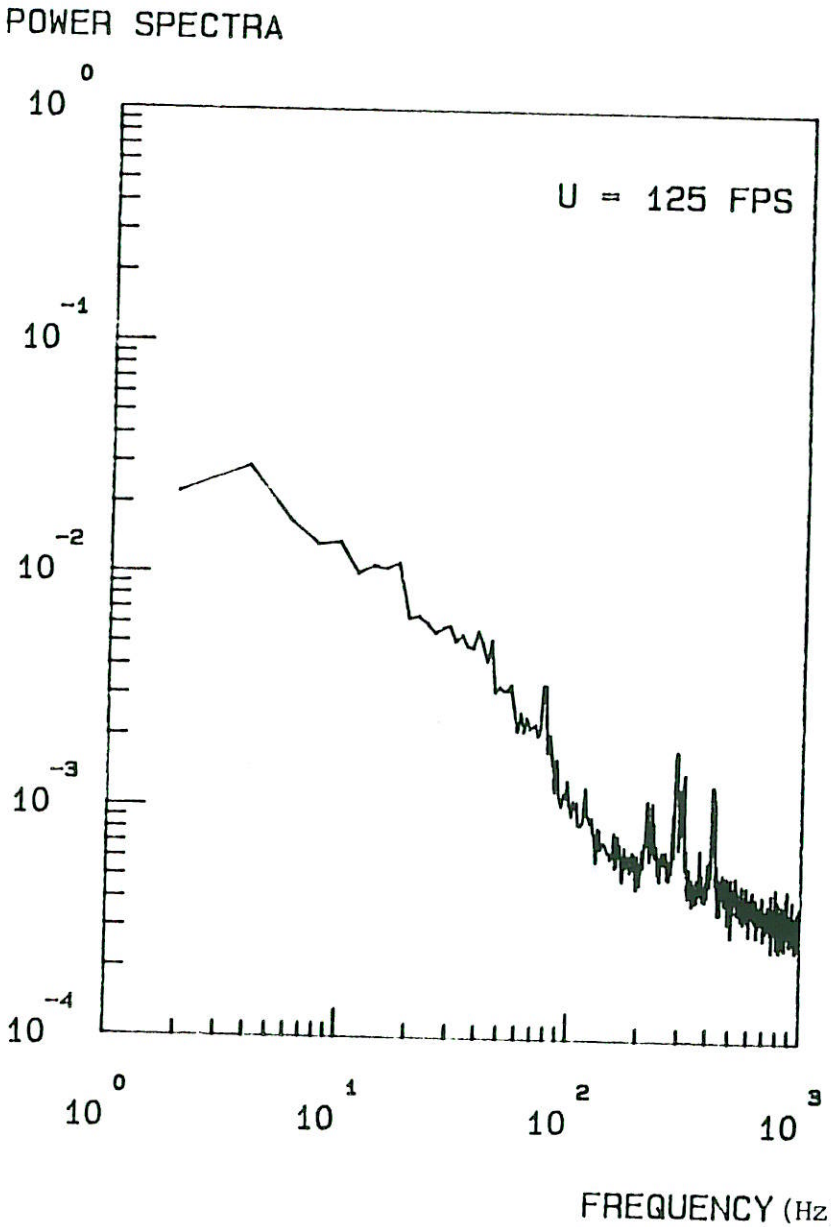

Fig. 7 f). Normalized power spectra at location B-3

$\overline{u^2}_{total}$=0.0207 fps^2, $\overline{u^2}_{turb}$=0.0136 fps^2

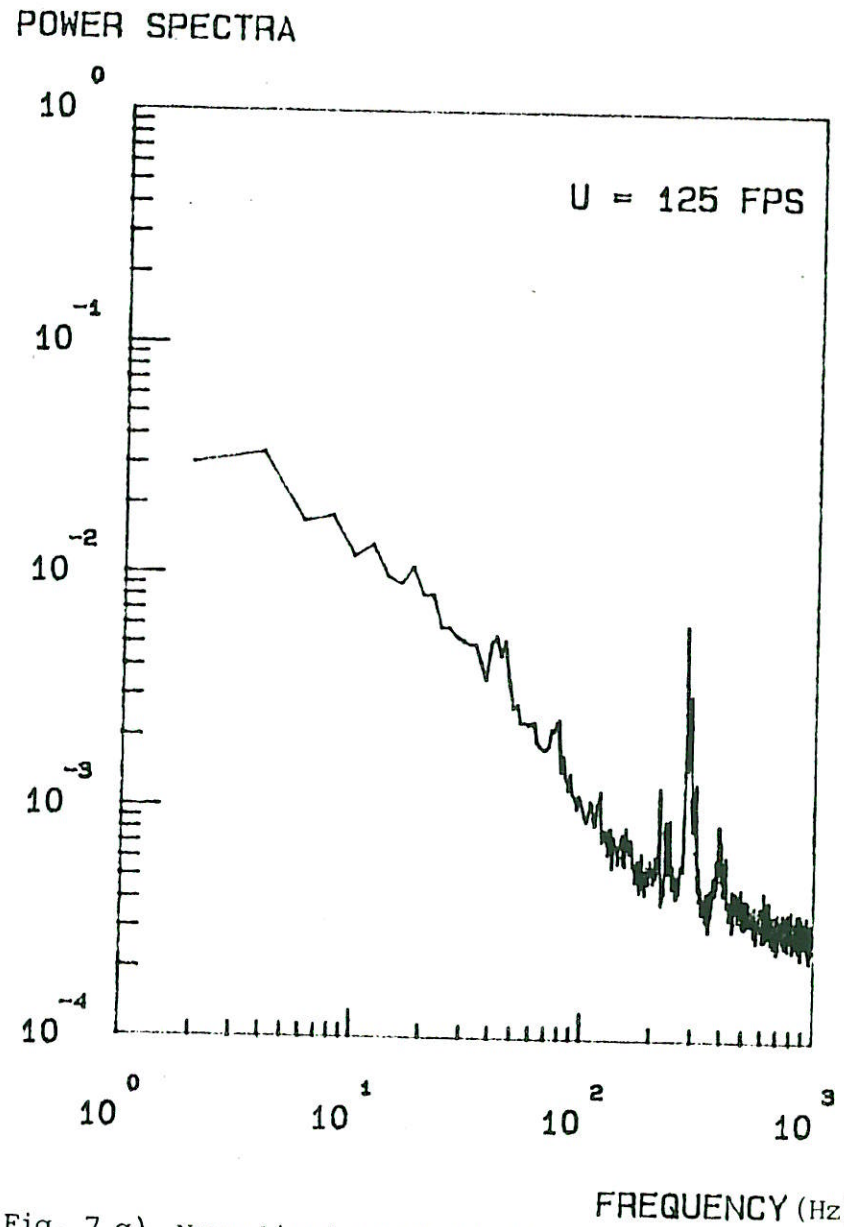

Fig. 7 g). Normalized power spectra at location C-1

$\overline{u^2}_{total}$=0.0233 fps^2, $\overline{u^2}_{turb}$=0.0160 fps^2

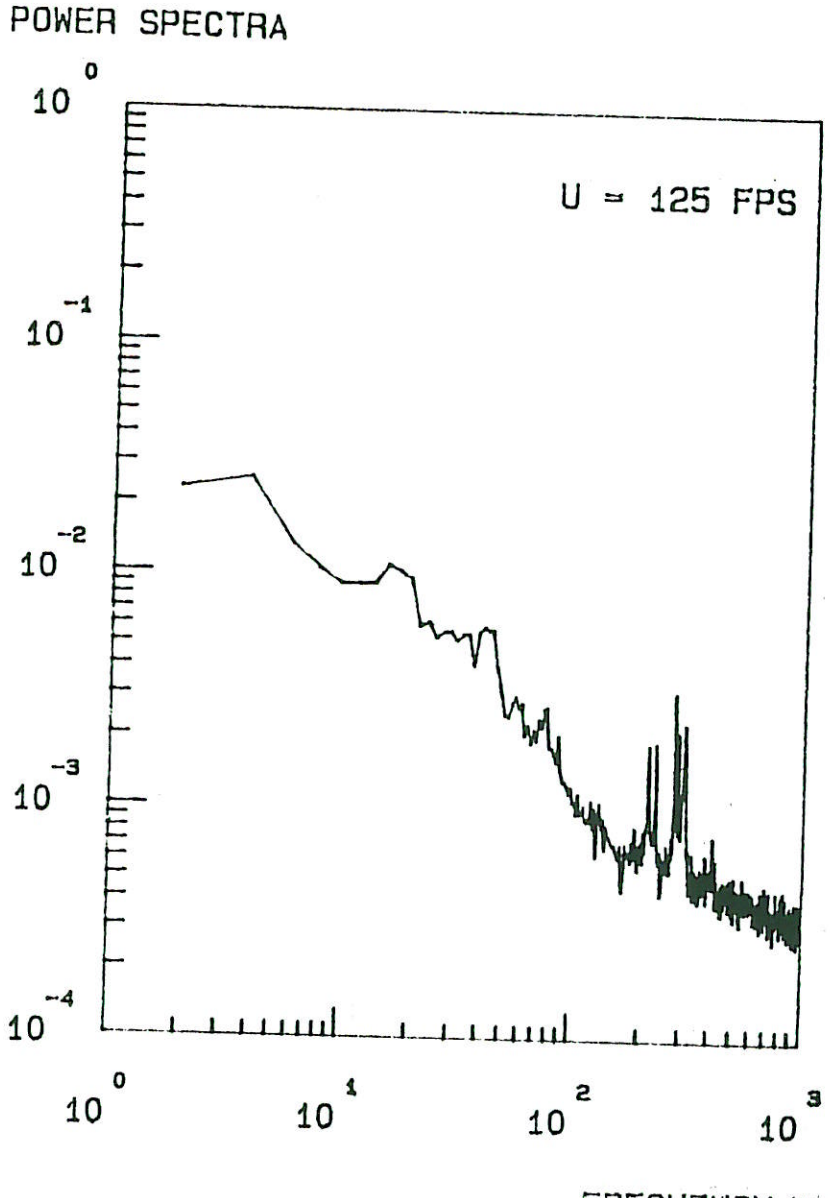

Fig. 7 h). Normalized power spectra at location C-2

$\overline{u^2}_{total}$=0.0247 fps^2, $\overline{u^2}_{turb}$=0.0169 fps^2